

Density-dependent nuclear interactions and the beta decay of ^{14}C : chiral three-nucleon forces and Brown-Rho scaling¹

J. W. Holt, N. Kaiser, and W. Weise

Physik Department, Technische Universität München,
D-85747 Garching, Germany

Abstract

We study the role of density-dependent low-momentum nucleon-nucleon interactions in describing the anomalously long beta decay lifetime of ^{14}C . We approach this problem both from the perspective of chiral effective field theory, in which genuine three-body forces generate an effective density-dependent two-body interaction, as well as from the perspective of Brown-Rho scaling, in which the masses and form factor cutoffs in one-boson-exchange interactions are modified in a dense nuclear medium due to the partial restoration of chiral symmetry. The beta decay transition of ^{14}C to the ground state of ^{14}N is calculated within the shell model using a model space consisting of two $0p$ -shell holes within a closed ^{16}O core. The effective $0p$ -shell interaction is calculated up to second order in perturbation theory with single-particle energies extracted from experiment. We find that both three-nucleon forces and Brown-Rho scaling medium modifications give qualitatively similar results not only for the ground state to ground state Gamow-Teller transition but also for Gamow-Teller transitions from excited states of ^{14}C to the ground state of ^{14}N . In this way, it is observed that at a low-momentum scale of $\Lambda_{\text{low-k}} = 2.1 \text{ fm}^{-1}$, medium-modifications of the nuclear force play an essential role in increasing the lifetime of ^{14}C from a few minutes to an archaeologically long one of 5730 years.

PACS: 21.30.Fe, 21.60.Cs, 23.40.-s

Keywords: Effective field theory at finite density, chiral three-nucleon force, Brown-Rho scaling, shell-model calculation of ^{14}C beta-decay.

1 Introduction

In recent years our understanding of nuclear structure physics, and the nuclear force in particular, has benefited greatly by incorporating aspects of the fundamental theory of strong interactions, QCD. Although QCD is highly nonperturbative at the energy scales characteristic for nucleons bound within nuclei, one can exploit the symmetry breaking pattern of QCD, namely the explicit and spontaneous breaking of chiral symmetry, to constrain the underlying effective theory for interacting nucleons. At low energies, this is accomplished through chiral effective field theory [1]–[10], in which the light pseudoscalar Nambu-Goldstone bosons (e.g. pions) generated by the spontaneous breaking of chiral symmetry comprise the low-energy mesonic degrees of freedom relevant for nuclear interactions. All other heavier mesons are integrated out and their effects are absorbed in a series of short-range contact interactions.

The above description utilizes the spontaneous breaking of chiral symmetry at low energies. However, as the temperature and/or density of a hadronic medium increases, the order parameter for chiral symmetry breaking (the scalar quark condensate $\langle \bar{q}q \rangle$) decreases in magnitude

¹Work supported in part by BMBF, GSI and by the DFG cluster of excellence: Origin and Structure of the Universe.

and is expected to vanish at an energy density around $1 \text{ GeV}/\text{fm}^3$, signaling the restoration of chiral symmetry. The vacuum structure of QCD, encoded in various quark and gluon condensates, is expected to play an important role in determining the properties (e.g. masses) of light hadrons [11]–[13], with the scalar quark condensate being of primary importance. The work of Brown and Rho [12, 14] was one of the first attempts to connect medium-dependent meson masses to the partial restoration of chiral symmetry as the temperature and/or density changes. By imposing scale invariance – a symmetry of classical, massless QCD – on chiral effective Lagrangians, Brown and Rho obtained a scaling law in which the masses of hadrons, except the pion, decrease with the cube root of the scalar quark condensate.

A natural testing ground for Brown-Rho scaling is heavy ion collisions, which produce hot/dense hadronic matter in the vicinity of chiral restoration. For a recent review see refs. [15, 16]. However, even for densities at the center of heavy nuclei, the scalar quark condensate is expected to decrease in magnitude by about 30% as found from model studies [17], low-density expansions [18], and calculations within in-medium chiral effective field theory [19]. The decreasing of meson masses at these densities would have important consequences for nuclear structure, since the intermediate-range attraction and strong short-distance repulsion in one-boson-exchange models of the nucleon-nucleon potential arise largely from the exchange of the σ and ω mesons, respectively. Moreover, phenomena that are sensitive to the tensor component of the nucleon-nucleon interaction would be affected by the decreasing of the ρ meson mass. It was therefore hoped that evidence for the partial restoration of chiral symmetry at finite density could already be found by studying the properties of normal nuclei.

Brown and Rho proposed employing the hidden local symmetry approach [20, 21] as a framework for studying mass scaling effects. In this formalism vector mesons, such as the ρ and ω , are treated as gauge bosons that acquire mass through the Higgs mechanism. Presently a consistent hidden local symmetry approach incorporating baryons has yet to be fully developed. This limits the applicability of the formalism to dense nuclear systems. A more practical approach has been to directly modify the masses of mesons in one-boson exchange interactions [22]–[26]. This leads to a density-dependent nucleon-nucleon interaction that can be used in nuclear structure studies. One aims to achieve a qualitative understanding of the effects of in-medium hadron masses on nuclear structure.

Not only can the mass of a hadron be affected by a background medium, but more generally the entire spectral function will be modified due to Pauli blocking effects, collisional broadening, and the opening of additional decay channels in a hadronic medium [27]–[31]. Indeed the study of spectral functions has become the dominant focus both experimentally and theoretically for probing the tendency towards chiral symmetry restoration below the transition point. The importance of resonance-hole excitations in modifying the spectral features of the vector mesons ρ and ω has been studied in detail.

Chiral effective field theory, representing the interface between QCD and nuclear physics at low energy and momentum scales, takes a different approach by integrating out mesons much heavier than pions. The short-distance dynamics is encoded in contact terms. Intermediate-range effects that would emerge from σ exchange and the ρ -exchange tensor force, are now generated by explicit two-pion exchange processes, subject to Pauli principle corrections in the nuclear medium. Resonance-hole effects are incorporated through genuine three-nucleon forces.

With the development of highly-accurate methods for solving the nuclear many-body problem for light nuclei, as well as infinitely-extended nuclear matter, it is now well established that free-space two-nucleon interactions alone are insufficient to describe the properties of dense nuclear systems. In particular, calculations using only nonrelativistic two-body forces have been unable to accurately reproduce the binding energies and spectra of light nuclei [32]–[34], the saturation binding energy and density of isospin-symmetric nuclear matter [35]–[39], and finally

the nucleon-deuteron scattering differential cross sections at intermediate energies [40]–[43]. In all of these cases, the errors arising from the solution of the nuclear many-body problem are small compared to the uncertainties in the underlying nuclear force model, which suggests the need to include explicitly degrees of freedom beyond nucleons and mesons, or equivalently the need to include three-body forces.

In this work we study the unique problem of the beta decay lifetime of ^{14}C , which has been shown [25, 44] to be highly sensitive to density-dependent effects in the nuclear interaction. Describing the beta decay lifetime of ^{14}C has long been a challenge in nuclear structure physics, because the anomalously small Gamow-Teller (GT) transition matrix element $M_{GT} \simeq 0.002$ results from the cancellation between terms that are otherwise on the order of 1. The valence particles of ^{14}C inhabit a region with a large nuclear density, and therefore medium modifications to the nucleon-nucleon interaction could be sizable. In ref. [25] it was suggested that a decreasing in-medium tensor force from Brown-Rho scaling plays a significant role in the suppression of the Gamow-Teller transition. This was inspired by early work [45, 46] that highlighted the sensitivity of the beta decay lifetime to the tensor component of the nuclear interaction. In contrast, a later study including three-nucleon forces [44] found qualitatively similar effects that resulted from additional short-distance repulsion coming from the contact three-body force. Within Brown-Rho-scaled nucleon-nucleon interaction models such an effect is generated by the decreasing of the ω meson mass. We wish to revisit the problem of the ^{14}C beta decay lifetime and suggest that, indeed, in both models of the low-momentum density-dependent nucleon-nucleon interaction, additional short-distance repulsion generates significant suppression of the Gamow-Teller transition.

This paper is organized as follows. In Section 2 we describe the framework of chiral effective field theory, and how a density-dependent two-nucleon force can be constructed from the chiral three-body interaction by summing over the filled Fermi sea of nucleons. In Section 3 we motivate Brown-Rho scaling and study the effect that such hadronic medium modifications have on the nuclear force. In Section 4 we apply both models to the problem of the extremely long beta decay lifetime of ^{14}C , which was suggested to be particularly sensitive to the density dependence of the nuclear force. We highlight the important role played by the short-distance repulsion (increasing with the nuclear density) in both approaches to the in-medium nuclear interaction. We end with a summary and conclusions.

2 Density-dependent nucleon-nucleon interaction from chiral effective field theory

Chiral effective field theory has proven to be a highly useful framework for studying the nuclear interaction problem (for current reviews, see refs. [10, 47]). By implementing the spontaneous and explicit breaking of chiral symmetry in QCD, one constructs a low-energy effective field theory of interacting pions and nucleons order-by-order in powers of Q/Λ_χ , where Q represents a nucleon momentum or the pion mass. The long- and intermediate-range parts of the nuclear force are generated by 1π , 2π (and more) exchange processes, whereas the short-distance dynamics due to heavy mesons and baryon resonances are integrated out and their effects are encoded in nucleon-nucleon contact terms. Currently the nuclear interaction has been calculated up to 4th order (N^3LO) in the chiral power counting [6]–[9]. It is at this order (and beyond) that it is possible to achieve an agreement with empirical NN scattering phase shifts that is comparable to previous high-precision NN potentials [48]–[50]. By adjusting the 29 parameters (mostly low-energy constants) that occur at this order, the 1999 database for np and pp elastic scattering up to $E_{\text{lab}} = 290$ MeV can be fit with a χ^2/dof of 1.1 for np scattering and

1.5 for pp scattering. Furthermore, the experimental deuteron binding energy, charge radius, and electric quadrupole moment are very well reproduced by the chiral N³LO potential [9].

One decisive practical advantage of the chiral effective field theory approach is that two- and many-body forces are generated consistently within the same framework. Chiral three-nucleon forces first appear at N²LO. There are three different components, which we show in diagrams (a), (b), and (c) in Fig. 1. The long-range, two-pion exchange interaction is given by

$$V_{3N}^{(2\pi)} = \sum_{i \neq j \neq k} \frac{g_A^2}{8f_\pi^4} \frac{\vec{\sigma}_i \cdot \vec{q}_i \vec{\sigma}_j \cdot \vec{q}_j}{(\vec{q}_i^2 + m_\pi^2)(\vec{q}_j^2 + m_\pi^2)} F_{ijk}^{\alpha\beta} \tau_i^\alpha \tau_j^\beta, \quad (1)$$

where $g_A = 1.27$, $f_\pi = 92.4$ MeV, $m_\pi = 138.04$ MeV is the average pion mass, $\vec{q}_i = \vec{p}_i' - \vec{p}_i$ is the difference between the final and initial momentum of nucleon i , and

$$F_{ijk}^{\alpha\beta} = \delta^{\alpha\beta} \left(-4c_1 m_\pi^2 + 2c_3 \vec{q}_i \cdot \vec{q}_j \right) + c_4 \epsilon^{\alpha\beta\gamma} \tau_k^\gamma \vec{\sigma}_k \cdot (\vec{q}_i \times \vec{q}_j). \quad (2)$$

The three low-energy constants of the long-range 3NF, namely $c_1 = -0.76$ GeV⁻¹, $c_3 = -4.78$ GeV⁻¹, and $c_4 = 3.96$ GeV⁻¹ appear in the two-pion exchange component of the NN interaction and therefore can be determined from fits to low-energy NN phase shifts [51]. The medium-range, one-pion exchange three-nucleon interaction is proportional to the low-energy constant c_D/Λ_χ and has the analytic form

$$V_{3N}^{(1\pi)} = - \sum_{i \neq j \neq k} \frac{g_A c_D}{8f_\pi^4 \Lambda_\chi} \frac{\vec{\sigma}_j \cdot \vec{q}_j}{\vec{q}_j^2 + m_\pi^2} \vec{\sigma}_i \cdot \vec{q}_i \vec{\tau}_i \cdot \vec{\tau}_j, \quad (3)$$

with $\Lambda_\chi = 700$ MeV. The filled black square in diagram (b) of Fig. 1 symbolizes the corresponding two-nucleon one-pion contact interaction. Finally, the short-distance contact three-body force is proportional to the low-energy constant c_E/Λ_χ and is given by

$$V_{3N}^{(\text{ct})} = \sum_{i \neq j \neq k} \frac{c_E}{2f_\pi^4 \Lambda_\chi} \vec{\tau}_i \cdot \vec{\tau}_j. \quad (4)$$

In eqs. (1)-(4) the nucleon labels i, j, k can take the values 1,2,3 which results in six possible permutations for each sum. The low-energy constants of the medium-range ($V_{3N}^{(1\pi)}$) and short-range ($V_{3N}^{(\text{ct})}$) three-body forces are fit to properties of few-nucleon systems, such as the triton binding energy together with the nd doublet scattering length [52], the ⁴He binding energy [53], or the binding energies and spectra of light nuclei [34]. The N³LO three-body interaction contains numerous one-loop diagrams but no additional low-energy constants and is currently under construction [47].

In this work we utilize renormalization group techniques to decimate the chiral N³LO two-body interaction down to an energy scale in the vicinity of $\Lambda = 2.0$ fm⁻¹, following the details provided in refs. [54, 55]. Such a decimation procedure has the desirable feature that the resulting “low-momentum interaction”, referred to as $V_{\text{low-k}}$, is nearly unique regardless of which underlying high-precision NN potential is employed, and therefore $V_{\text{low-k}}$ provides a model-independent description of the nucleon-nucleon interaction below $\Lambda = 2.0$ fm⁻¹. The analogous evolution of realistic three-body forces down to this scale has yet to be achieved. However, since such a decimation would change primarily the short-distance part of the three-body interaction, a practical alternative has been to treat the low-energy constants c_D and c_E as functions of the variable $\Lambda_{\text{low-k}}$. By fitting $c_D(\Lambda_{\text{low-k}})$ and $c_E(\Lambda_{\text{low-k}})$ to the binding energies of ³H and ⁴He, one obtains [56] the values shown in Table 1 for two different choices of the low-momentum cutoff.

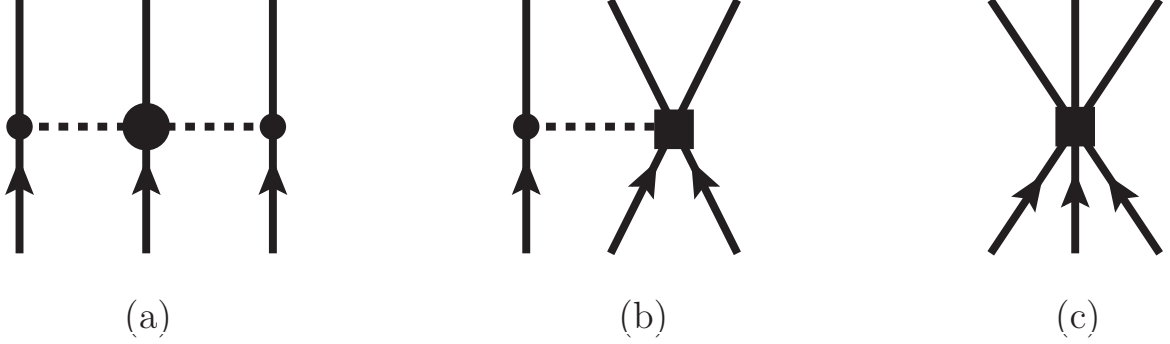


Figure 1: The leading-order contributions to the chiral three-nucleon force: (a) the long-range 2π -exchange force $V_{3N}^{(2\pi)}$, (b) the medium-range 1π -exchange force $V_{3N}^{(1\pi)}$, and (c) the short-range contact interaction $V_{3N}^{(ct)}$.

$\Lambda_{\text{low-k}}$	c_D	c_E
2.1 fm^{-1}	-2.062	-0.625
2.3 fm^{-1}	-2.785	-0.822

Table 1: The values of the low-energy constants c_D and c_E of the chiral three-nucleon interaction fit to the binding energies of $A = 3, 4$ nuclei for different values of the momentum cutoff $\Lambda_{\text{low-k}}$.

We now show how to derive from the leading-order chiral three-nucleon interaction, eqs. (1–4), an effective density-dependent in-medium NN interaction. We keep our discussion brief and refer the interested reader to the original references [44, 57]. We consider the on-shell scattering of two nucleons in isospin-symmetric (spin-saturated) nuclear matter of density $n = 2k_f^3/3\pi^2$ in the center-of-mass frame, $N_1(\vec{p}) + N_2(-\vec{p}) \rightarrow N_1(\vec{p} + \vec{q}) + N_2(-\vec{p} - \vec{q})$, where k_f is the Fermi momentum. The magnitude of the in- and out-going nucleon momenta is $|\vec{p}| = p = |\vec{p} + \vec{q}|$, and $q = |\vec{q}|$ is the magnitude of the momentum transfer. The resulting interaction in momentum-space has the following (general) form

$$\begin{aligned}
V(\vec{p}, \vec{q}) &= V_C + \vec{\tau}_1 \cdot \vec{\tau}_2 W_C + [V_S + \vec{\tau}_1 \cdot \vec{\tau}_2 W_S] \vec{\sigma}_1 \cdot \vec{\sigma}_2 + [V_T + \vec{\tau}_1 \cdot \vec{\tau}_2 W_T] \vec{\sigma}_1 \cdot \vec{q} \vec{\sigma}_2 \cdot \vec{q} \\
&+ [V_{SO} + \vec{\tau}_1 \cdot \vec{\tau}_2 W_{SO}] i(\vec{\sigma}_1 + \vec{\sigma}_2) \cdot (\vec{q} \times \vec{p}) \\
&+ [V_Q + \vec{\tau}_1 \cdot \vec{\tau}_2 W_Q] \vec{\sigma}_1 \cdot (\vec{q} \times \vec{p}) \vec{\sigma}_2 \cdot (\vec{q} \times \vec{p}).
\end{aligned} \tag{5}$$

The subscripts refer to the central (C), spin-spin (S), tensor (T), spin-orbit (SO), and quadratic spin orbit (Q) components of the NN interaction, each of which occurs in an isoscalar (V) and an isovector (W) version.

In Figs. 2 and 3 we show the six topologically distinct contributions to the in-medium density-dependent nucleon-nucleon interaction to one-loop order. The long-range two-pion exchange three-nucleon force generates the diagrams shown in Fig. 2. Tadpole diagrams obtained by contracting the in- and outgoing lines at a πNN vertex vanish, which leaves only three topologically distinct nonvanishing contributions. The short double-line on a nucleon propagator symbolizes the filled Fermi sea of nucleons, which introduces the “medium insertion” $-2\pi\delta(k_0)\theta(k_f - |\vec{k}|)$ in the in-medium nucleon propagator. Diagram (1) in Fig. 2 represents one-pion exchange with a Pauli-blocked pion self-energy correction. The intermediate nucleon momentum is independent of the momentum transfer \vec{q} carried by the pions and therefore

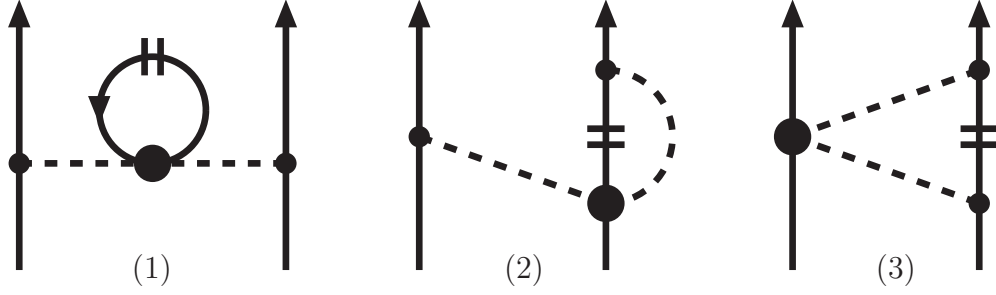


Figure 2: In-medium NN interaction generated by the two-pion exchange component of the chiral three-nucleon interaction. The short double-line symbolizes the filled Fermi sea of nucleons. Reflected diagrams of (2) and (3) are not shown.

the integration over the filled Fermi sea of nucleons produces a correction proportional to the density n :

$$V_{NN}^{\text{med},1} = \frac{g_A^2 M_N n}{8\pi f_\pi^4} \vec{\tau}_1 \cdot \vec{\tau}_2 \frac{\vec{\sigma}_1 \cdot \vec{q} \vec{\sigma}_2 \cdot \vec{q}}{(m_\pi^2 + q^2)^2} (2c_1 m_\pi^2 + c_3 q^2). \quad (6)$$

Since $c_{1,3} < 0$, this term gives a (large) enhancement of the bare 1π -exchange:

$$V_{NN}^{(1\pi)} = -\frac{g_A^2 M_N}{16\pi f_\pi^2} \vec{\tau}_1 \cdot \vec{\tau}_2 \frac{\vec{\sigma}_1 \cdot \vec{q} \vec{\sigma}_2 \cdot \vec{q}}{m_\pi^2 + q^2}. \quad (7)$$

In part this enhancement can be interpreted in terms of the reduced in-medium pion decay constant, $f_{\pi,s}^{*2} = f_\pi^2 + 2c_3\rho$, which is associated with the spatial components of the axial current. Diagram (2) of Fig. 2 represents a vertex correction to one-pion exchange. Fermi sphere integrals, $\int_{|\vec{k}|\leq k_F} d^3k$, over a single static pion propagator give rise to p -dependent functions $\Gamma_j(p)$, where the dependence on k_F is implicit. For the sake of brevity and continuity in the current discussion, we have left the explicit expressions for the $\Gamma_j(p)$ in the Appendix. Summing diagram (2) of Fig. 6 together with the three reflected diagrams yields the following contribution

$$V_{NN}^{\text{med},2} = \frac{g_A^2 M_N}{32\pi^3 f_\pi^4} \vec{\tau}_1 \cdot \vec{\tau}_2 \frac{\vec{\sigma}_1 \cdot \vec{q} \vec{\sigma}_2 \cdot \vec{q}}{m_\pi^2 + q^2} \left\{ -4c_1 m_\pi^2 [\Gamma_0(p) + \Gamma_1(p)] \right. \\ \left. - (c_3 + c_4) [q^2 (\Gamma_0(p) + 2\Gamma_1(p) + \Gamma_3(p)) + 4\Gamma_2(p)] + 4c_4 \left[\frac{2k_f^3}{3} - m_\pi^2 \Gamma_0(p) \right] \right\}. \quad (8)$$

By analyzing the momentum- and density-dependent factors in eq. (8) relative to $V_{NN}^{(1\pi)}$, one finds that this contribution corresponds to a (large) reduction of the 1π -exchange in the nuclear medium. Approximately, this feature can be interpreted in terms of a quenched nucleon axial-vector constant g_A^* .

Diagram (3) in Fig. 2 represents Pauli-blocked 2π -exchange. The Fermi sphere integrals over two pion propagators give rise to p - and q -dependent functions $G_j(p, q)$ which we tabulate in the Appendix. Diagram (3) taken together with the corresponding reflected diagram then produces the contribution

$$V_{NN}^{\text{med},3} = \frac{g_A^2 M_N}{64\pi^3 f_\pi^4} \left\{ -12c_1 m_\pi^2 [2\Gamma_0(p) - (2m_\pi^2 + q^2)G_0(p, q)] \right. \\ \left. - c_3 [8k_f^3 - 12(2m_\pi^2 + q^2)\Gamma_0(p) - 6q^2\Gamma_1(p) + 3(2m_\pi^2 + q^2)^2 G_0(p, q)] \right. \\ \left. + 4c_4 \vec{\tau}_1 \cdot \vec{\tau}_2 (\vec{\sigma}_1 \cdot \vec{\sigma}_2 q^2 - \vec{\sigma}_1 \cdot \vec{q} \vec{\sigma}_2 \cdot \vec{q}) G_2(p, q) \right\}$$

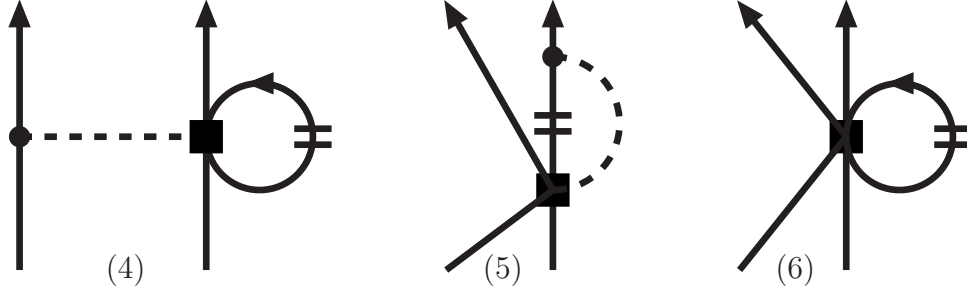


Figure 3: In-medium NN interaction generated by the one-pion exchange component and the short-range component of the chiral three-nucleon interaction.

$$\begin{aligned}
& -(3c_3 + c_4 \vec{\tau}_1 \cdot \vec{\tau}_2) i(\vec{\sigma}_1 + \vec{\sigma}_2) \cdot (\vec{q} \times \vec{p}) \left[2\Gamma_0(p) + 2\Gamma_1(p) - (2m_\pi^2 + q^2) \right. \\
& \times \left(G_0(p, q) + 2G_1(p, q) \right) \left. \right] - 12c_1 m_\pi^2 i(\vec{\sigma}_1 + \vec{\sigma}_2) \cdot (\vec{q} \times \vec{p}) \left[G_0(p, q) + 2G_1(p, q) \right] \\
& \left. + 4c_4 \vec{\tau}_1 \cdot \vec{\tau}_2 \vec{\sigma}_1 \cdot (\vec{q} \times \vec{p}) \vec{\sigma}_2 \cdot (\vec{q} \times \vec{p}) \left[G_0(p, q) + 4G_1(p, q) + 4G_3(p, q) \right] \right\}. \quad (9)
\end{aligned}$$

In comparison to the analogous 2π -exchange interaction in vacuum (see section 4.2 in ref. [58]) the Pauli blocking in the nuclear medium has generated additional spin-orbit terms, $i(\vec{\sigma}_1 + \vec{\sigma}_2) \cdot (\vec{q} \times \vec{p})$, and quadratic spin-orbit terms, $\vec{\sigma}_1 \cdot (\vec{q} \times \vec{p}) \vec{\sigma}_2 \cdot (\vec{q} \times \vec{p})$, written in the last three lines of eq. (9).

Next we consider the 1π -exchange component of the chiral three-nucleon interaction proportional to the parameter c_D/Λ_χ . Contracting two external lines results in two (nonvanishing) topologies. By closing a nucleon line at the contact vertex, one obtains a vertex correction to 1π -exchange:

$$V_{NN}^{\text{med},4} = -\frac{g_A M_N c_D n}{32\pi f_\pi^4 \Lambda_\chi} \vec{\tau}_1 \cdot \vec{\tau}_2 \frac{\vec{\sigma}_1 \cdot \vec{q} \vec{\sigma}_2 \cdot \vec{q}}{m_\pi^2 + q^2}. \quad (10)$$

We note that this contribution is proportional to the nuclear density n due to the q -independent Fermi sphere integral. Since c_D is negative, $V_{NN}^{\text{med},4}$ reduces the bare 1π -exchange, roughly by about 16% at normal nuclear matter density $\rho_0 = 0.16 \text{ fm}^{-3}$. Diagram (5) in Fig. 3 represents Pauli-blocked (pionic) vertex corrections to the short-range NN interaction. The corresponding contribution to the density dependent in-medium NN interaction reads:

$$\begin{aligned}
V_{NN}^{\text{med},5} = & \frac{g_A M_N c_D}{64\pi^3 f_\pi^4 \Lambda_\chi} \left\{ \vec{\tau}_1 \cdot \vec{\tau}_2 \left[2\vec{\sigma}_1 \cdot \vec{\sigma}_2 \Gamma_2(p) + \left(\vec{\sigma}_1 \cdot \vec{\sigma}_2 \left(2p^2 - \frac{q^2}{2} \right) + \vec{\sigma}_1 \cdot \vec{q} \vec{\sigma}_2 \cdot \vec{q} \left(1 - \frac{2p^2}{q^2} \right) \right. \right. \right. \\
& \left. \left. \left. - \frac{2}{q^2} \vec{\sigma}_1 \cdot (\vec{q} \times \vec{p}) \vec{\sigma}_2 \cdot (\vec{q} \times \vec{p}) \right) \left(\Gamma_0(p) + 2\Gamma_1(p) + \Gamma_3(p) \right) \right] + 4k_f^3 - 6m_\pi^2 \Gamma_0(p) \right\} \quad (11)
\end{aligned}$$

Due to the special spin and isospin structure of this term, it gives nonvanishing contributions only to relative S -states as well as to the ${}^3S_1 - {}^3D_1$ mixing matrix element.

Finally, we discuss the short-range component of the chiral 3N interaction, represented by a three-nucleon contact-vertex proportional to c_E/Λ_χ . By closing one nucleon line (see diagram (6) in Fig. 3) one obtains the following contribution to the in-medium NN-interaction:

$$V_{NN}^{\text{med},6} = -\frac{3M_N c_E n}{8\pi f_\pi^4 \Lambda_\chi}, \quad (12)$$

which simply grows linearly in density n and is independent of spin, isospin and nucleon momenta.

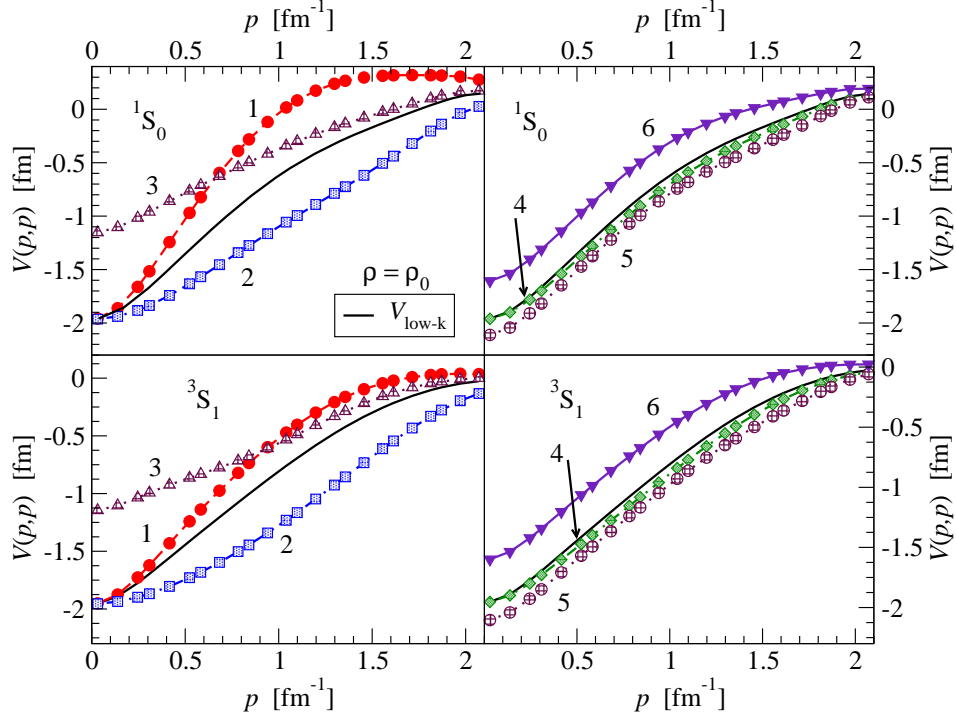


Figure 4: Effect (at normal nuclear matter density, $n_0 = 0.16 \text{ fm}^{-3}$) of the six different terms $V_{NN}^{\text{med},i}$ on the S -wave components of the free-space nucleon-nucleon potential $V_{\text{low-}k}$ for a low-momentum cutoff of $\Lambda_{\text{low-}k} = 2.1 \text{ fm}^{-1}$.

In Fig. 4 we show the contribution from each of these components of the density-dependent NN interaction to the 1S_0 and 3S_1 diagonal partial wave matrix elements (see ref. [57] for an analysis of higher partial waves). The black solid line gives the matrix elements of $V_{\text{low-}k}$ obtained from the Idaho N³LO chiral NN potential for a momentum cutoff of $\Lambda_{\text{low-}k} = 2.1 \text{ fm}^{-1}$. The various curves labeled $i = 1, 2, \dots, 6$ show the matrix elements of $V_{\text{low-}k} + V_{NN}^{\text{med},i}$. We see that the effects from the long-range two-pion exchange part of the chiral three-nucleon force are quite large. However, the pion self-energy correction $V_{NN}^{\text{med},1}$ largely cancels the effects of the vertex correction $V_{NN}^{\text{med},2}$. Since $V_{NN}^{\text{med},1}$ and $V_{NN}^{\text{med},2}$ are simply modifications to one-pion exchange, a similar cancellation occurs in all higher partial waves as well. The final component, $V_{NN}^{\text{med},3}$, that comes from the long-range three-body force has a much richer spin and isospin structure, and at large distances (small momenta) the overall effect is strongly repulsive.

The two terms $V_{NN}^{\text{med},4}$ and $V_{NN}^{\text{med},5}$ arise from the medium-range one-pion exchange three-body force proportional to the low-energy constant c_D . In Fig. 4 we see that the effects are much weaker than from the long-range chiral three-nucleon force. Since $V_{NN}^{\text{med},4}$ is again just a reduction of one-pion exchange, it has nonzero contributions in all partial waves. The second term arising from the mid-range three-nucleon force, $V_{NN}^{\text{med},5}$, is also relatively small and gives an additional (equal) attraction in the two relative S -states, as well as the coupled $^3S_1 - ^3D_1$ mixing matrix element not shown in the figure. The final contribution $V_{NN}^{\text{med},6}$ is a pure contact interaction and therefore contributes only to the two relative S -states. The interaction is spin and isospin independent and therefore contributes to both of these partial waves equally. Indeed, the additional repulsion is approximately twice as large as the attraction coming from $V_{NN}^{\text{med},5}$, so taking these two terms together essentially results in a weaker short-range repulsive interaction.

In Fig. 5 we show the density dependence (for $n = 0, n_0/2$, and n_0) of the diagonal S -wave matrix elements of $V_{\text{low-}k} + V_{NN}^{\text{med}}$. Overall, we find that the effects are repulsive and quite large in comparison to the free-space low-momentum NN interaction. The same holds in most higher partial waves as well, with the exception that the tensor component of the in-medium interaction becomes more attractive with the density [57]. The large S -wave repulsion in the three-body forces increases with the density and thereby provides the mechanism for saturation of low-momentum interactions [59]. In Section 4 we study the role that these density-dependent effects play in describing the anomalously long beta decay lifetime of ^{14}C and make a comparison with analogous interactions obtained from the Brown-Rho scaling hypothesis.

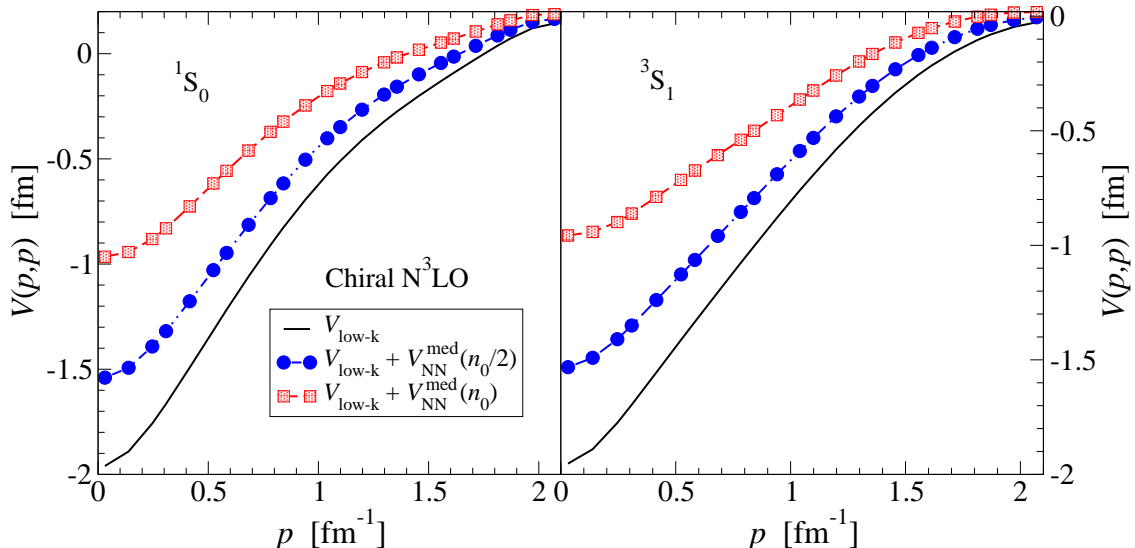


Figure 5: Partial wave matrix elements for relative S -states from $V_{\text{low-}k} + V_{NN}^{\text{med}}$. The low-momentum decimation scale is taken to be $\Lambda_{\text{low-}k} = 2.1 \text{ fm}^{-1}$.

3 Brown-Rho scaled nucleon-nucleon interactions

In this section we summarize Brown-Rho scaling and describe a model approach for implementing these effects in nuclear interactions at densities close to that of saturated nuclear matter. The starting point is the scaling relation for (light) hadron masses derived by Brown and Rho [12]:

$$\sqrt{\frac{g_A}{g_A^*} \frac{M_N^*}{M_N}} \simeq \frac{m_\sigma^*}{m_\sigma} \simeq \frac{m_\rho^*}{m_\rho} \simeq \frac{m_\omega^*}{m_\omega} \simeq \frac{f_\pi^*}{f_\pi} = \Phi(n), \quad (13)$$

which was obtained by implementing scale invariance in chiral effective Lagrangians following the approach of Campbell et al. [60]. In eq. (13) the asterisk refers to an in-medium value of the given quantity, $f_\pi^* = f_{\pi,t}^*$ is related to the time component of the axial vector current, and Φ (to be discussed in more detail shortly) is a function of the nuclear density n . Absent from the scaling hypothesis in eq. (13) is the pion mass, which in the chiral limit of massless bare quarks would be zero due to the Goldstone boson nature of pions. The nonzero pion mass is due rather to the explicit breaking of chiral symmetry by the quark mass term in the QCD

Lagrangian and is therefore not as sensitive to the background medium as are the masses of other hadrons. This is supported empirically from measurements of energy shifts in deeply bound pionic atoms [61, 62].

From eq. (13), hadronic masses are predicted to scale with the pion decay constant f_π , the hadronic observable connected to the spontaneous breaking of chiral symmetry. The connection between f_π and the fundamental order parameter $\langle \bar{q}q \rangle$ of QCD is given by the Gell-Mann–Oakes–Renner relation [63, 17]

$$f_\pi^2 m_\pi^2 = -m_q \langle \bar{u}u + \bar{d}d \rangle, \quad (14)$$

where m_q is the average (current) mass for up u and down d quarks. Assuming that the pion mass is protected by chiral invariance, this relation would produce

$$\frac{f_\pi^*}{f_\pi} = \left(\frac{\langle \bar{q}q \rangle^*}{\langle \bar{q}q \rangle} \right)^{1/2}, \quad (15)$$

where $\langle \bar{q}q \rangle^* = \langle \Omega | \bar{q}q | \Omega \rangle$ and $|\Omega\rangle$ denotes the ground state of the dense medium. In the limit of low densities the scalar quark condensate is related to the nuclear density by [18, 64]

$$\frac{\langle \bar{q}q \rangle^*}{\langle \bar{q}q \rangle} = 1 - \frac{\sigma_{\pi N}}{f_\pi^2 m_\pi^2} n + \dots, \quad (16)$$

where $\sigma_{\pi N}$ is the pion-nucleon sigma term that describes how the nucleon mass varies with the masses of bare quarks. From a dispersion relation analysis of low-energy πN scattering, one can deduce $\sigma_{\pi N} \simeq 45$ MeV [65]. Thus, at nuclear matter saturation density one would obtain from eqs. (13), (15), and (16) that $\Phi(n_0) \simeq 0.83$. In Brown-Rho scaling one therefore assumes a linear decrease of hadronic mass with the density:

$$\frac{m^*}{m} \simeq 1 - \frac{1}{2} \frac{\sigma_{\pi N}}{f_\pi^2 m_\pi^2} n \simeq 1 - 0.17 \frac{n}{n_0}. \quad (17)$$

Such a relationship has also been deduced from in-medium QCD sum rule analyses, which can provide important constraints on the form of the vector meson spectral functions [13, 28, 66].

Brown-Rho scaling was one of the first attempts to study – through changes in the symmetry breaking pattern of the ground state – the effects of a hot/dense medium on the properties of an embedded hadron. Subsequent work had the broader goal to obtain the full spectral function of in-medium hadrons, with special emphasis on the vector mesons: ρ and ω . Within hadronic many-body calculations, self-energy corrections Σ_{med} to the meson propagator $D(\omega, \vec{q})$ defined by

$$D(\omega, \vec{q}) = \frac{1}{\omega^2 - \vec{q}^2 - m^2 - \Sigma_{\text{vac}}(q) - \Sigma_{\text{med}}(\omega, \vec{q})} \quad (18)$$

result in modifications to the spectral function $A(\omega, \vec{q})$, which is proportional to the imaginary part of the propagator:

$$A(\omega, \vec{q}) = \frac{1}{\pi} \frac{\text{Im} \Sigma(\omega, \vec{q})}{(\omega^2 - \vec{q}^2 - m^2 + \text{Re} \Sigma(\omega, \vec{q}))^2 + \text{Im} \Sigma^2(\omega, \vec{q})}. \quad (19)$$

The real part of the self-energy then contributes to the effective mass of the particle while the imaginary part leads to collisional broadening of the width. In a background medium of cold nuclear matter, contributions to Σ_{med} arise from the coupling of mesons to nucleon-hole and resonance-hole excitations [30, 28, 67, 68] as shown in Fig. 6(a). Calculations are simplified by invoking the following general result that holds at low-densities (corresponding to small

Fermi momenta) and which relates the in-medium self-energy to the total forward scattering amplitude $T(\vec{q}, \omega)$ of a vector meson on a nucleon

$$\Sigma_{\text{med}}(\omega, \vec{q}) = \int_{p_N < k_f} \frac{d^3 p_N}{(2\pi)^3 2E_N} T(q, p_N) \simeq \frac{n}{8m_N} T(\vec{q}, \omega), \quad (20)$$

where n is the nucleon density and one assumes that the scattering amplitude varies slowly with momentum. The result of such studies was that medium modifications to vector meson spectral functions in nuclear matter are dominated by subthreshold resonances, such as the $D_{13}(1520)$ resonance which produces an enhancement in the low-energy region of the ρ and ω meson spectral functions. Most calculations concluded that the spectral functions of vector mesons in cold nuclear matter are largely broadened with little shift of the peak mass. However, within an in-medium QCD sum rule approach it has been found [66] that the first moment of the ρ -meson spectral function can decrease (similarly to that in eq. (13)) despite the fact that the mass peak changes very little.

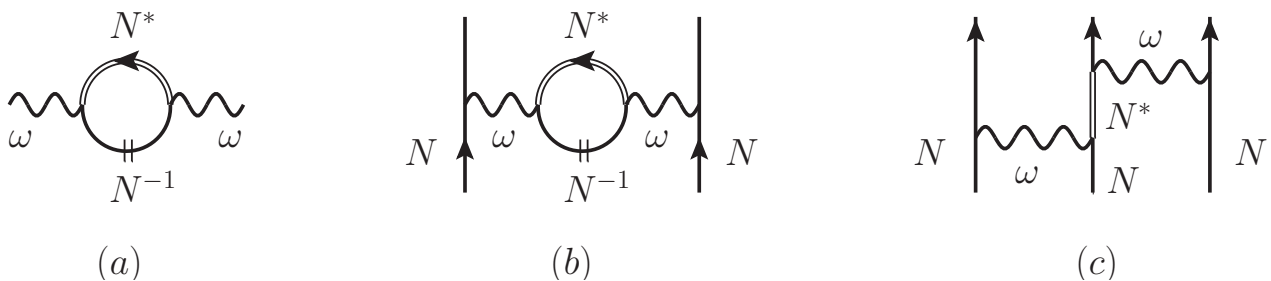


Figure 6: The contribution of resonance-hole excitations to (a) the in-medium ω meson propagator, (b) the in-medium NN interaction resulting from ω meson exchange, and (c) the analogous contribution to the three-nucleon force.

Three-nucleon forces and hadronic medium modifications provide two complementary (and partly equivalent) frameworks for understanding and implementing density-dependence in the nucleon-nucleon interaction. The role of baryonic resonances are important for each: on the one hand they give rise to genuine three-nucleon forces, and on the other hand they provide the main mechanism for altering mesonic spectral functions in medium. The connection can be visualized in the three diagrams of Fig. 6, which show (a) a process contributing to the modification of the ω -meson spectral function in medium, (b) the effect that such a process would have on the one-boson-exchange NN interaction due to ω meson exchange, and (c) the corresponding three-nucleon force obtained by opening the nucleon hole line in diagram (b). At present chiral three-nucleon forces are better constrained experimentally and provide a complete basis for including effects of the medium, while the properties of hadrons in medium are less constrained but have a more direct connection to questions regarding chiral symmetry restoration in dense nuclear systems. In the rest of this section we consider a specific model for implementing Brown-Rho scaling medium modifications in one-boson-exchange interactions in order to make a quantitative comparison to models of the density-dependent NN interaction from chiral three-nucleon forces.

The scaling relation in eq. (13) should be regarded as only an approximate, mean-field relation that could be altered through higher-order corrections. Indeed, it is well-established [22, 23] that a naive implementation of eq. (13) would yield far too much attraction due to the

decreasing of the effective scalar σ meson mass. A more accurate treatment of the intermediate-range attraction in the NN potential would be to replace the “fictitious” σ meson by a pair of correlated pions (in the $J^\pi = 0^+$ channel). This has been done in ref. [69], where a meson exchange model for the S -wave $\pi\pi$ interaction was developed and found to be dominated by the exchange of the ρ meson as well as repulsive $\pi\pi$ contact interactions constrained by chiral symmetry. With this model for the $\pi\pi$ interaction, the $\pi\pi \rightarrow N\bar{N}$ amplitude was then constructed, which can be related through crossing relations and a dispersion integral to the $\pi N \rightarrow \pi N$ amplitude from which one can derive the effective 2π -exchange NN potential.

n/n_0	m_{σ_1} (MeV)	$g_{\sigma_1}^2/4\pi$	m_{σ_2} (MeV)	$g_{\sigma_2}^2/4\pi$
0.0	640	4.36	377	0.640
0.5	538	3.41	295	0.450
0.75	471	2.88	249	0.309
1.0	395	2.53	220	0.264
1.25	365	2.35	200	0.234

Table 2: Masses and coupling constants for the two zero-width bosons parameterizing medium-modified correlated 2π exchange in the Bonn-B potential. [23]

In this formalism finite density effects in the scalar-isoscalar channel arise through the density-dependence of the ρ meson mass (m_ρ) and form factor cutoff (Λ_ρ) as well as the $\pi\pi$ contact interactions. Moreover, the in-medium pion propagator is dressed with Δ -hole excitations. In practice, this complicated treatment of correlated 2π exchange was modeled with the exchange of two scalar-isoscalar bosons with a form factor cutoff of $\Lambda_\sigma = 3$ GeV and masses and coupling constants shown in Table 2. Together with the scaling of the vector meson masses and form factor cutoffs², namely

$$\frac{m_\rho^*}{m_\rho} = \frac{m_\omega^*}{m_\omega} = \frac{\Lambda^*}{\Lambda} = 1 - 0.15 \frac{n}{n_0}, \quad (21)$$

the modifications to correlated 2π exchange form the basis of the in-medium Bonn-B potential [23]. The potential includes also the exchange of the π , η , and a_0 mesons as described in ref. [71]. Using this model of the medium-modified (MM) Bonn-B potential, the properties of symmetric nuclear matter were studied [23], and it was found that medium effects in scalar-isoscalar exchange diminished with increasing density, thereby allowing for a reasonable description of nuclear saturation in a Dirac-Brueckner-Hartree-Fock calculation.

In Fig. 7 we show the on-shell matrix elements of the low-momentum MM Bonn-B potential in relative S -waves for three different densities: $n = \{0, n_0/2 \text{ and } n_0\}$. In comparison to the S -wave matrix elements found for the density-dependent chiral interaction, we see that the main difference lies in the low-momentum components of the interaction. Whereas the Pauli-blocked two-pion exchange diagram in Fig. 3 gives rise to a large repulsion at low momenta (see Fig. 5), the dropping of the effective σ_1 and σ_2 masses in the MM Bonn-B potential increases the medium- and long-range attraction. Indeed, at nuclear matter saturation density, the effective σ meson masses have dropped to 395 and 220 MeV (from 640 and 377 MeV respectively), which extends the range of the attraction significantly. This enhanced attraction is partially mitigated by a simultaneous drop in the effective coupling constants g_{σ_1} and g_{σ_2} . However,

²To the extent that the phenomenological form factors associated nucleon-meson interaction vertices are governed by the nucleon radius, they too will decrease with density due to the proposed increase in the nucleon size [70].

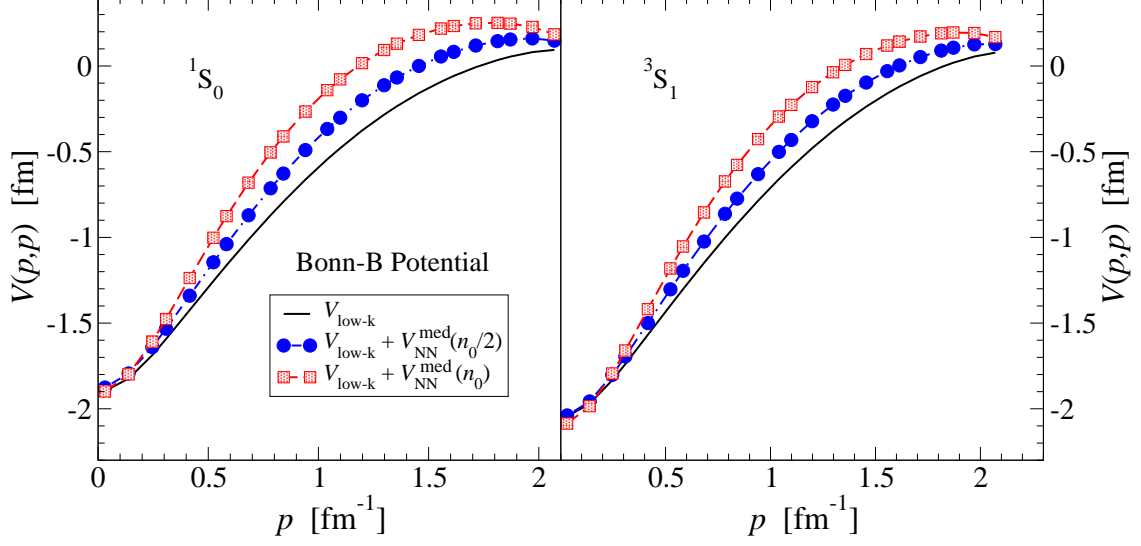


Figure 7: Diagonal matrix elements for relative S waves obtained from the low-momentum medium-modified Bonn-B potential at three densities: $n = \{0, n_0/2, n_0\}$.

at higher momenta we see that the two theories lead to similar modifications in the S -wave interactions. In the density-dependent chiral interaction the short-range contact interaction proportional to c_E provides most of the additional repulsion, whereas in the MM Bonn-B potential an analogous effect is achieved through the dropping of the ω meson mass.

One of the original motivations for studying the beta decay of ^{14}C within the framework of Brown-Rho scaling was the sensitivity of the Gamow-Teller matrix element to the nuclear tensor force. In fact, employing a residual interaction consisting of only central and spin-orbit forces it is not possible to achieve a vanishing matrix element in a pure two p -hole configuration [45]. Jancovici and Talmi [46] showed that by including a strong tensor force one could construct an interaction which reproduces the lifetime of ^{14}C as well as the magnetic moment and electric quadrupole moment of ^{14}N , although agreement with the known spectroscopic data was unsatisfactory. The most important contributions to the tensor component of the nuclear potential arise from π and ρ meson exchange, which have opposite signs:

$$\begin{aligned}
 V_\rho^T(r) &= -\frac{f_{N\rho}^2}{4\pi} m_\rho \vec{\tau}_1 \cdot \vec{\tau}_2 S_{12} \left[\frac{1}{(m_\rho r)^3} + \frac{1}{(m_\rho r)^2} + \frac{1}{3m_\rho r} \right] e^{-m_\rho r}, \\
 V_\pi^T(r) &= \frac{f_{N\pi}^2}{4\pi} m_\pi \vec{\tau}_1 \cdot \vec{\tau}_2 S_{12} \left[\frac{1}{(m_\pi r)^3} + \frac{1}{(m_\pi r)^2} + \frac{1}{3m_\pi r} \right] e^{-m_\pi r},
 \end{aligned} \tag{22}$$

where $S_{12} = 3\vec{\sigma}_1 \cdot \hat{r} \vec{\sigma}_2 \cdot \hat{r} - \vec{\sigma}_1 \cdot \vec{\sigma}_2$ is the tensor operator and $f_{N\pi} = g_A m_\pi / 2f_\pi$. Since the ρ meson mass is expected to decrease substantially at nuclear matter density while the pion mass remains relatively constant, an unambiguous prediction of Brown-Rho scaling is the decreasing of the total tensor force at finite density. However, as we show in the next section, the additional short-range repulsive force resulting from the decreasing ω meson mass also plays an important role in suppressing the associated Gamow-Teller strength.

4 Beta decay lifetime of ^{14}C

The extremely long half-life of ^{14}C ($T_{1/2} \simeq 5730$ yr [72]) plays an essential role in archaeological dating methods, yet naively one would expect the lifetime to be nearly six orders of magnitude smaller. The 0^+ ground state of ^{14}C and the 1^+ ground state of ^{14}N to which it decays satisfy the selection for allowed Gamow-Teller transitions, and according to the Wigner spin-isospin $\text{SU}(4)$ symmetry for light nuclei the associated transition matrix element would be unity. However, in order to reproduce the experimentally observed lifetime, the Gamow-Teller transition matrix element must be approximately $2 \cdot 10^{-3}$, which is expected to result from an accidental cancellation among otherwise large terms. This transition therefore provides a sensitive test for nuclear interaction models and many-body methods.

Early studies with phenomenological interactions highlighted the importance of the nuclear tensor force, without which it would not be possible to obtain a vanishing Gamow-Teller matrix element in a $0p^{-2}$ model space [45, 46]. Employing realistic NN interaction models did not improve the theoretical description significantly [73], but the use of larger model spaces in no-core shell model calculations appeared to generally diminish the Gamow-Teller matrix element [74]. Despite the long history of the problem, it was only recently suggested that the beta decay lifetime is particularly sensitive to the density-dependence of the nuclear force [25, 44]. The first of these studies employed the medium modified Bonn-B potential, described in the previous section, while the latter made use of the density-dependent chiral NN interaction constructed in Section 2. Indeed, since ^{14}C and ^{14}N lie just below the double shell-closure at ^{16}O , the density in the vicinity of the valence nucleons is fairly large. In Fig. 8 we plot twice the charge distribution of ^{14}N obtained from electron scattering experiments [75, 76] fit to the harmonic oscillator density distribution

$$n(r) \propto \left(1 + b \frac{r^2}{d^2}\right) e^{-r^2/d^2}, \quad (23)$$

where for ^{14}N , $b = 1.29$ and $d = 1.74$ fm. Also plotted in the same figure is the square of the radial $0p$ wavefunction which peaks at a radius where the nucleon density is close to 90% that of saturated nuclear matter $n_0 = 0.16 \text{ fm}^{-3}$. The rest of this section is devoted to a systematic comparison between the two models of the in-medium nuclear interaction, which despite several qualitative differences in their density dependence, both predict that the beta decay transition of ^{14}C is strongly suppressed by medium effects in the nuclear force.

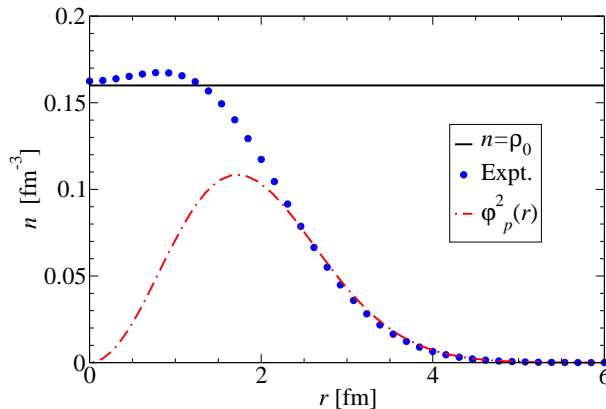


Figure 8: Twice the charge distribution of ^{14}N taken from [75, 76] together with the square of the radial $0p$ -shell wavefunctions.

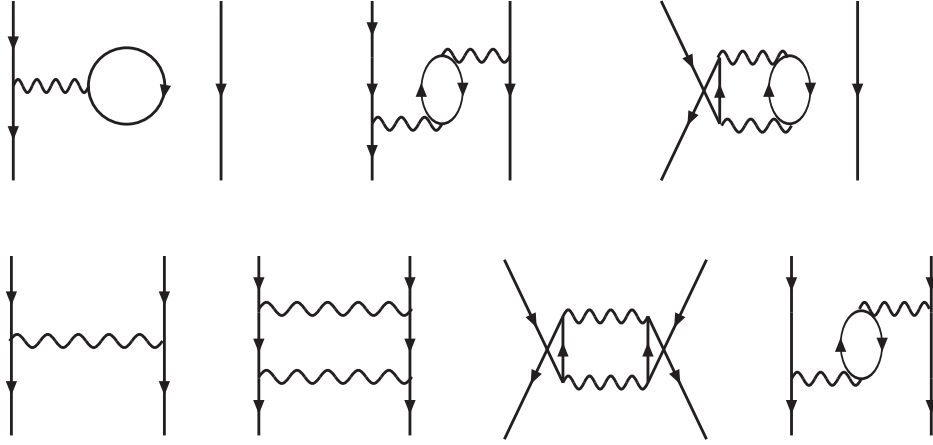


Figure 9: Diagrams contributing to the effective interaction V_{eff} in our present calculation. Wavy lines represent the density-dependent in-medium nuclear interaction calculated in Sections 2 and 3.

Nuclei with mass number $A > 13$ are currently beyond the reach of ab-initio methods, such as the no-core shell model [77] and quantum Monte Carlo techniques [78]. We approach this problem from shell model perturbation theory using a model space consisting of two $0p$ holes in a closed ^{16}O core. The many-body Schrödinger equation

$$H\Psi_n = E_n\Psi_n, \quad (24)$$

is replaced by the model space equation

$$H_{\text{eff}}\chi_m = E_m\chi_m, \quad (25)$$

where $H_{\text{eff}} = H_0 + V_{\text{eff}}$ and H_0 is the sum of the kinetic energy and the harmonic oscillator single particle potential with oscillator parameter $\hbar\omega = 14$ MeV. We derive the shell model effective interaction V_{eff} following the formalism explained in refs. [79, 80]. The effective interaction is constructed from a folded diagram expansion in the so-called \hat{Q} -box, which consists of all irreducible valence-linked diagrams (usually truncated to a given order). In the present calculation we include hole-hole diagrams in the \hat{Q} -box up to second-order in perturbation theory, shown in Fig. 9. In this figure the wavy line represents the full interaction, either $V_{\text{low-}k} + V_{NN}^{\text{med}}$ or the low-momentum medium-modified Bonn-B potential, $V_{\text{Bonn-B}}^{\text{med}}$. Finally, we need the energy splitting between the two $0p$ orbitals, $\epsilon = e(p_{1/2}) - e(p_{3/2})$, which is most accurately obtained from the experimental excitation energy of the first $3/2^-$ state of ^{15}N located 6.3 MeV above the $1/2^-$ ground state.

We denote the relevant single-hole states by

$$|1\rangle = |0s_{1/2}^{-1}\rangle, |2\rangle = |0p_{3/2}^{-1}\rangle, |3\rangle = |0p_{1/2}^{-1}\rangle, \quad (26)$$

and the two-hole states coupled to good angular momentum J , isospin T , and parity π are denoted by $|\alpha\beta; J^\pi T\rangle$, where $\alpha, \beta = 2$ or 3 . After constructing the effective interaction with the folded diagram method, we diagonalize the following matrix to obtain the eigenvalues and eigenstates with $J^\pi = 1^+, T = 0$ (relevant for ^{14}N):

$$\begin{bmatrix} \vdots & & & \\ \cdots & \langle\alpha\beta; 1^+0|V_{\text{eff}}|\gamma\delta; 1^+0\rangle & \cdots & \\ \vdots & & & \end{bmatrix} + \begin{bmatrix} 0 & 0 & 0 \\ 0 & -\epsilon & 0 \\ 0 & 0 & -2\epsilon \end{bmatrix}, \quad (27)$$

For the $J^\pi = 0^+, T = 1$ states, we diagonalize a similar 2×2 matrix. The ground states for ^{14}C and ^{14}N are the lowest $J^\pi = 0^+, T = 1$ and $J^\pi = 1^+, T = 0$ states respectively, which we denote by

$$\begin{aligned}\psi_i &= a |22; 0^+1\rangle + b |33; 0^+1\rangle, \\ \psi_f &= x |22; 1^+0\rangle + y |23; 1^+0\rangle + z |33; 1^+0\rangle.\end{aligned}\quad (28)$$

From these wavefunctions one can derive the following expression for the reduced Gamow-Teller matrix element M_{GT} :

$$M_{GT} = \sum_k \langle \psi_f | \sigma(k) \tau_+(k) | \psi_i \rangle = \frac{1}{\sqrt{6}} \left(-2\sqrt{5}ax + 2\sqrt{2}ay + 4by + 2bz \right), \quad (29)$$

where experimentally $M_{GT} \simeq 2 \cdot 10^{-3}$.

For orientation we first determine the low-lying states of ^{14}C and ^{14}N , as well as the Gamow-Teller transition matrix element connecting the two ground states, using the free-space low-momentum N^3LO potential at a resolution scale of $\Lambda_{\text{low-}k} = 2.1 \text{ fm}^{-1}$. We will see shortly that there is only a small difference when using the free-space Bonn-B potential. For the two 0^+ states of ^{14}C we find

$$\begin{aligned}\psi_1(0^+, 1) &= 0.396 |22; 0^+, 1\rangle + 0.918 |33; 0^+, 1\rangle, \\ \psi_2(0^+, 1) &= 0.918 |22; 0^+, 1\rangle - 0.396 |33; 0^+, 1\rangle,\end{aligned}\quad (30)$$

with energy splitting $\Delta E(0^+) = 12.9 \text{ MeV}$. For the two lowest 1^+ states we find

$$\begin{aligned}\psi_1(1^+, 0) &= 0.142 |22; 0^+, 1\rangle - 0.681 |23; 0^+, 1\rangle + 0.719 |33; 0^+, 1\rangle, \\ \psi_2(1^+, 0) &= 0.361 |22; 0^+, 1\rangle - 0.663 |23; 0^+, 1\rangle - 0.656 |33; 0^+, 1\rangle,\end{aligned}\quad (31)$$

where the first excited state lies $\Delta E(1^+) = 2.76 \text{ MeV}$ above the ground state. The second excited $J^\pi = 1^+, T = 0$ state lies nearly 16 MeV higher in energy than the ground state and will therefore be neglected throughout. With these wavefunctions, the ground state to ground state Gamow-Teller transition matrix element is found to be

$$M_{GT} = -0.90, \quad (32)$$

which is much too large to describe the known lifetime of ^{14}C . From the ground state wavefunctions in eqs. (30) and (31) we see that the first three terms in eq. (29) add coherently while the last gives a contribution of the opposite sign, though not enough to cancel the first three. In order for medium effects to suppress the transition, strength must therefore be shifted to the $|33\rangle$ component of both ground state wavefunctions.

We now implement density-dependence in the nuclear potential and study the effect on the model space interaction matrix elements. In Tables 3 and 4 we show the shell model matrix elements for the low-momentum interactions derived from the in-medium chiral N^3LO and Brown-Rho-scaled (BRS) Bonn-B potentials both in free space and at nuclear matter saturation density. Table 3 shows the matrix elements for the $J^\pi = 0^+, T = 1$ states, while Table 4 shows the matrix elements for the $J^\pi = 1^+, T = 0$ states. Overall, medium effects in both potentials lead to qualitatively similar changes in the shell model matrix elements, though the density-dependence of the in-medium chiral interaction is much stronger. This should not be surprising, given the stronger S -wave repulsion in the in-medium chiral interaction, as compared to the BRS Bonn-B potential, shown in Figs. 4 and 7.

$$J^\pi = 0^+, T = 1$$

n/n_0	$\langle 22 V_{\text{Chiral}}^{\text{med}} 22\rangle$	$\langle 22 V_{\text{Chiral}}^{\text{med}} 33\rangle$	$\langle 33 V_{\text{Chiral}}^{\text{med}} 33\rangle$
0	-3.28	-3.77	-0.61
0.25	-2.64	-3.66	-0.05
1.0	-0.12	-2.88	1.91

n/n_0	$\langle 22 V_{\text{Bonn}}^{\text{med}} 22\rangle$	$\langle 22 V_{\text{Bonn}}^{\text{med}} 33\rangle$	$\langle 33 V_{\text{Bonn}}^{\text{med}} 33\rangle$
0	-3.12	-3.65	-0.54
0.25	-2.72	-3.38	-0.33
1.0	-1.09	-2.21	0.48

Table 3: Matrix elements (in units of MeV) between $0p^{-2}$ states coupled to $(J^\pi, T) = (0^+, 1)$ for the in-medium chiral interaction as well as the Brown-Rho-scaled Bonn-B potential at three different densities: $n = 0, 0.25n_0$, and n_0 .

$$J^\pi = 1^+, T = 0$$

n/n_0	$\langle 22 V_{\text{Chiral}}^{\text{med}} 22\rangle$	$\langle 23 V_{\text{Chiral}}^{\text{med}} 22\rangle$	$\langle 23 V_{\text{Chiral}}^{\text{med}} 23\rangle$	$\langle 23 V_{\text{Chiral}}^{\text{med}} 33\rangle$	$\langle 22 V_{\text{Chiral}}^{\text{med}} 33\rangle$	$\langle 33 V_{\text{Chiral}}^{\text{med}} 33\rangle$
0.0	-1.19	3.89	-5.20	1.36	1.66	-1.67
0.25	-0.61	3.74	-4.81	1.50	1.33	-1.00
1.0	1.29	2.81	-3.03	1.92	0.44	0.72

n/n_0	$\langle 22 V_{\text{Bonn}}^{\text{med}} 22\rangle$	$\langle 23 V_{\text{Bonn}}^{\text{med}} 22\rangle$	$\langle 23 V_{\text{Bonn}}^{\text{med}} 23\rangle$	$\langle 23 V_{\text{Bonn}}^{\text{med}} 33\rangle$	$\langle 22 V_{\text{Bonn}}^{\text{med}} 33\rangle$	$\langle 33 V_{\text{Bonn}}^{\text{med}} 33\rangle$
0.0	-1.28	3.50	-4.91	1.23	1.46	-1.68
0.25	-1.09	3.27	-4.56	1.24	1.38	-1.57
1.0	-0.31	2.31	-3.11	1.26	1.04	-1.09

Table 4: Matrix elements (in units of MeV) between $0p^{-2}$ states coupled to $(J^\pi, T) = (1^+, 0)$ for the in-medium chiral interaction as well as the Brown-Rho-scaled Bonn-B potential at three different densities: $n = 0, 0.25n_0$, and n_0 .

At nuclear matter saturation density, medium effects on both potentials are quite large. Nevertheless, we can gain insight by studying the interactions at low densities and employing perturbation theory. One finds the following corrections to the ground state wavefunctions:

$$\begin{aligned} \psi_1^{(1)}(0^+, 1) &= \psi_1^{(0)}(0^+, 1) - \frac{1}{12.9} \left[0.36\langle 22|V^{\text{med}}|22\rangle + 0.69\langle 22|V^{\text{med}}|33\rangle \right. \\ &\quad \left. - 0.36\langle 33|V^{\text{med}}|33\rangle \right] \psi_2^{(0)}(0^+, 1) \end{aligned} \quad (33)$$

and

$$\begin{aligned} \psi_1^{(1)}(1^+, 0) &= \psi_1^{(0)}(1^+, 0) - \frac{1}{2.76} \left[0.05\langle 22|V^{\text{med}}|22\rangle - 0.34\langle 23|V^{\text{med}}|22\rangle + 0.45\langle 23|V^{\text{med}}|23\rangle \right. \\ &\quad \left. - 0.03\langle 23|V^{\text{med}}|33\rangle + 0.17\langle 22|V^{\text{med}}|33\rangle - 0.47\langle 33|V^{\text{med}}|33\rangle \right] \psi_2^{(0)}(1^+, 0). \end{aligned} \quad (34)$$

A straightforward calculation using the matrix elements shown in Tables 3 and 4 for $n = 0.25n_0$ gives for the un-normalized perturbed wavefunctions arising from $V_{\text{Chiral}}^{\text{med}}$

$$\psi_0^{(1)}(0^+, 1) = \psi_0^{(0)}(0^+, 1) - 0.01\psi_1^{(0)}(0^+, 1) \quad \text{and}$$

	In-medium chiral N ³ LO						In-medium Bonn-B					
n/n_0	a	b	x	y	z	M_{GT}	a	b	x	y	z	M_{GT}
0.0	0.40	0.92	0.14	-0.68	0.72	-0.90	0.40	0.93	0.11	-0.62	0.78	-0.70
0.2	0.38	0.92	0.15	-0.69	0.71	-0.91	0.35	0.94	0.08	-0.55	0.83	-0.49
0.4	0.36	0.93	0.14	-0.67	0.73	-0.82	0.32	0.95	0.05	-0.50	0.86	-0.32
0.6	0.33	0.94	0.13	-0.65	0.75	-0.74	0.29	0.96	0.03	-0.45	0.89	-0.17
0.8	0.30	0.96	0.12	-0.62	0.78	-0.64	0.25	0.97	0.02	-0.40	0.92	-0.04
1.0	0.26	0.97	0.11	-0.59	0.80	-0.53	0.21	0.98	0.01	-0.36	0.93	0.07

Table 5: The coefficients of the jj -coupled wavefunctions defined in eq. (28) and the associated reduced GT matrix element as a function of the nuclear density n for both the Brown-Rho-scaled Bonn-B potential and the in-medium chiral nuclear interaction.

$$\psi_0^{(1)}(1^+, 0) = \psi_0^{(0)}(1^+, 0) + 0.04\psi_1^{(0)}(1^+, 0), \quad (35)$$

We see that a positive $\langle 22; 0^+1 | V^{\text{med}} | 22; 0^+1 \rangle$ and a positive $\langle 22; 0^+1 | V^{\text{med}} | 33; 0^+1 \rangle$ lead to a stronger $|33; 0^+, 1\rangle$ component in the perturbed ^{14}C ground state wavefunction. One therefore expects quite generally that additional density-dependent repulsion would increase the $|33; 0^+1\rangle$ component in the ^{14}C ground state and therefore help suppress the beta decay of ^{14}C . Both the in-medium chiral nuclear interaction and the BRS Bonn-B potential share this feature.

For the ground state of ^{14}N the situation is more complicated due to the larger number of terms in the perturbed wavefunction of eq. (34) as well as the more complicated dependence of the shell model matrix elements on the perturbing potential. The two dominant terms are $\langle 33; 1^+0 | V^{\text{med}} | 33; 1^+0 \rangle$ and $\langle 23; 1^+0 | V^{\text{med}} | 23; 1^+0 \rangle$, which have the same sign as the perturbing potential in S -waves but enter with opposite sign in the perturbed wavefunction. At one-quarter of nuclear matter density, the sum of all six contributions to $V_{\text{Chiral}}^{\text{med}}$ yields $\langle 33; 1^+0 | V_{\text{Chiral}}^{\text{med}} | 33; 1^+0 \rangle = 0.67$ MeV and $\langle 23; 1^+0 | V_{\text{Chiral}}^{\text{med}} | 23; 1^+0 \rangle = 0.39$ MeV. The remaining four terms together give a minute contribution to the perturbed wavefunction, and therefore we expect at low densities for the $|33; 1^+, 0\rangle$ component in the ground state of ^{14}N to decrease for the in-medium chiral interaction and consequently increase the magnitude of the Gamow-Teller transition matrix element. Since different components of the in-medium chiral interaction have different density-dependences, this behavior can change at higher densities. Indeed by inspecting the shell model matrix elements at nuclear matter saturation density we see that the opposite effect occurs and the GT matrix element is suppressed rather than enhanced (the perturbing potential is quite large and therefore our argument based on perturbation theory should be treated cautiously). In contrast, the BRS Bonn-B potential has $\langle 33; 1^+0 | V_{\text{Bonn}}^{\text{med}} | 33; 1^+0 \rangle = 0.11$ MeV and $\langle 23; 1^+0 | V_{\text{Bonn}}^{\text{med}} | 23; 1^+0 \rangle = 0.35$ MeV, which suggests that even at low densities the beta decay should be suppressed.

We now consider the results of the full calculation, including all density-dependent contributions to second-order in the shell model effective interaction shown in Fig. 9. In Table 5 we show the results of our calculations for the expansion coefficients of the ground state wavefunctions of ^{14}C and ^{14}N , as well as the reduced GT matrix element, as a function of the nuclear density up to $n = n_0$. The full results agree well with the conclusions we obtained from arguments based on perturbation theory. The Gamow-Teller transition matrix element decreases immediately at low densities in the BRS Bonn-B potential, while only after $n \simeq 0.25n_0$ do the density-dependent corrections of the chiral nuclear interaction lead to a suppression of the matrix element.

The Gamow-Teller transition strength, $B(GT)$, is related to the reduced GT transition matrix element by

$$B(GT) = (g_A^*)^2 \frac{1}{2J_i + 1} |M_{GT}|^2 \simeq |M_{GT}|^2, \quad (36)$$

where $J_i = 0$ and we have used the approximation that the in-medium axial vector coupling constant $g_A^* \simeq 1$. In general, the effective Gamow-Teller operator has additional terms in a nuclear medium [81, 82]:

$$\vec{\mathcal{O}}_{GT,eff} = g_{LA} \vec{L} + g_A^* \vec{\sigma} + g_{PA} [Y_2, \vec{\sigma}], \quad (37)$$

where \vec{L} is the orbital angular momentum operator and Y_2 denotes the rank-2 spherical harmonic $Y_{2,m}$. However, from theoretical calculations [83] of the effective GT operator in-medium, as well as beta decay calculations [84] performed with phenomenological shell model effective interactions, it is known that g_{LA} and g_{PA} are almost negligible and that in light nuclei g_A^* is smaller by 15-20% from its free space value of $g_A = 1.27$ (measured in free neutron beta decay). In general, one must calculate both the effective interaction V_{eff} and the effective Gamow-Teller operator $\vec{\mathcal{O}}_{GT,eff}$. In our calculations we assume a 20% reduction of g_A in medium and therefore set $g_A^* = 1.0$.

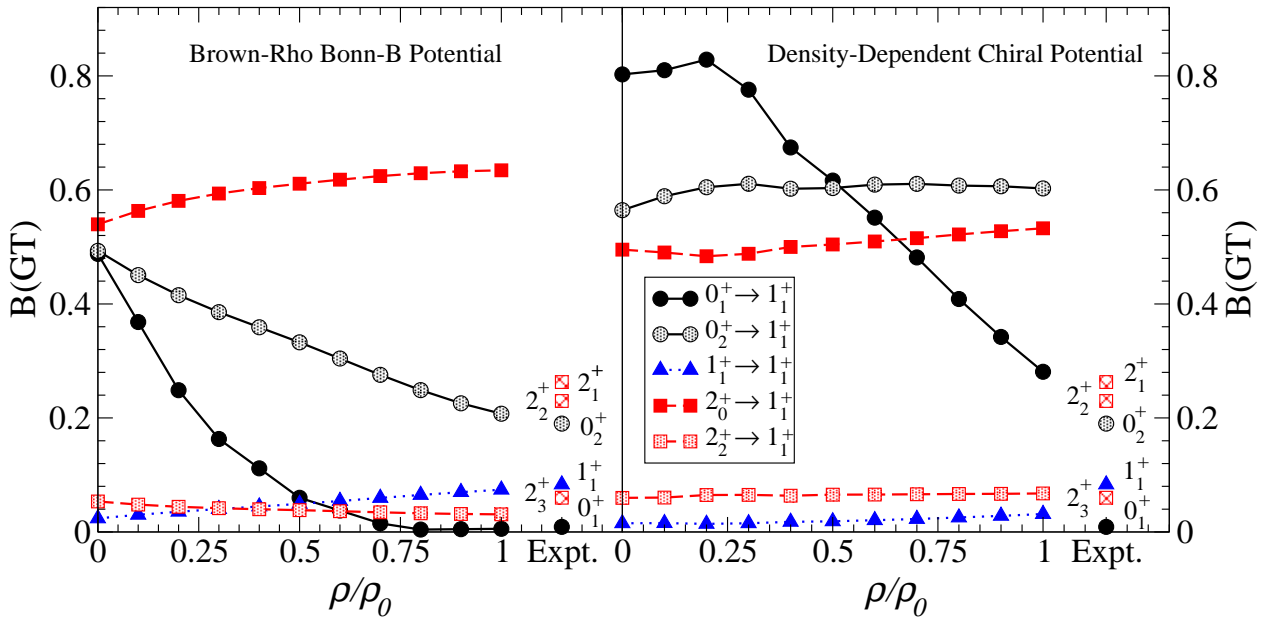


Figure 10: The $B(GT)$ values for transitions from low-lying states of ^{14}C to the ground state of ^{14}N as a function of the nuclear density. The experimental values are from [85]. Note that there are three experimental low-lying 2^+ states compared to two theoretical 2^+ states in the $0p^{-2}$ shell model configuration.

In Fig. 10 we plot the $B(GT)$ strengths for transitions from the low-lying states of ^{14}C to the ground state of ^{14}N for both density-dependent NN interactions. These are compared to the experimental values [85] obtained from the charge-exchange reaction $^{14}\text{N}(d, ^2\text{He})^{14}\text{C}$. From Fig. 10 one sees that the most dramatic effect is a reduction in the ground state to ground state Gamow-Teller transition strength in both models. In the Brown-Rho-scaled Bonn-B potential also the first excited $(0^+, 1)$ state of ^{14}C is decreased toward the experimental value.

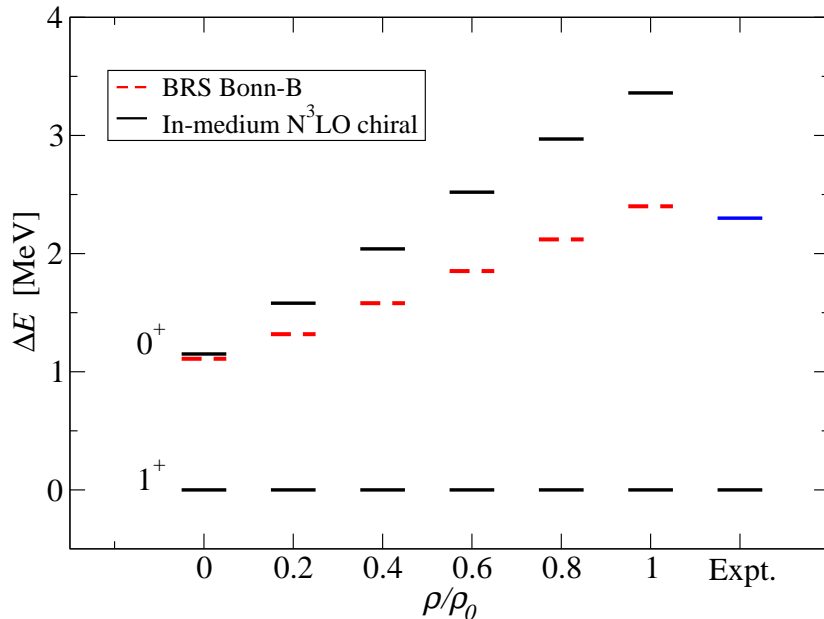


Figure 11: The splitting between the 1^+ ground state of ^{14}N and the first excited 0^+ state as a function of the nuclear density for both the medium-modified Bonn-B potential and the in-medium chiral nuclear interaction. Also shown is the experimental energy splitting $\Delta E_{0^+ - 1^+} = 2.3$ MeV.

Such an effect can be obtained from in-medium chiral interactions, but only if the strength of the contact three-body force is increased [44]. In the present version of the in-medium chiral nuclear interaction, there appears to be very little effect on the other Gamow-Teller transition strengths.

Besides comparing the Gamow-Teller strengths within the two models, it is useful to study the energy splitting between the ground state of ^{14}N and the first excited $(0^+, 1)$ state (the isobaric analogue of the ^{14}C ground state), which is experimentally observed to lie at 2.3 MeV. In Fig. 11 we plot this energy splitting as a function of the nuclear density for the in-medium chiral nuclear interaction and the BRS Bonn-B potential. It is clear that free-space nucleon-nucleon interactions systematically underpredict this level splitting and that additional density-dependent repulsion leads to an enhancement of the splitting. The in-medium chiral nuclear interaction is much more repulsive than the BRS Bonn-B potential and therefore leads to a larger increase in the splitting which overpredicts the value at higher densities. Nevertheless, we find that qualitatively the two models for the density-dependent NN interaction are consistent with one another and improve the agreement with experiment.

In order to better understand the relationship between the in-medium chiral nuclear interaction and the BRS Bonn-B potential, we first study in detail the six different one-loop contributions to V_{NN}^{med} arising from the leading-order chiral three-nucleon force. In Tables 6 and 7 we show the most important shell model matrix elements for each of these components at nuclear matter saturation density n_0 . Again, we let perturbation theory arguments direct our attention to the relevant physics. As previously mentioned, in order to suppress the Gamow-

Teller transition matrix element, it is necessary to increase the $|33; J^\pi T\rangle$ components of the ground state wavefunctions for both ^{14}C and ^{14}N . From eq. (33) it follows that only $V_{\text{NN}}^{\text{med},1}$, $V_{\text{NN}}^{\text{med},3}$, and $V_{\text{NN}}^{\text{med},6}$ contribute in the desired way. The remaining three contributions to $V_{\text{NN}}^{\text{med}}$ are attractive and decrease the strength of the $|33; 0^+, 1\rangle$ component of the ^{14}C ground state wavefunction. The structure of the ^{14}N perturbed ground state is most strongly affected by the $\langle 33; 1^+0|V^{\text{med}}|33; 1^+0\rangle$ and $\langle 23; 1^+0|V^{\text{med}}|23; 1^+0\rangle$ matrix elements. A secondary role is played by the $\langle 22; 1^+0|V^{\text{med}}|23; 1^+0\rangle$ and $\langle 22; 1^+0|V^{\text{med}}|33; 1^+0\rangle$ components. From Table 7 we see that out of the three contributions that shift strength to the $|33; 0^+1\rangle$ component of the ^{14}C ground state, only the three-nucleon contact interaction proportional to c_E also strongly shifts strength to the $|33; 1^+0\rangle$ component of ^{14}N :

$$\begin{aligned}
V_{\text{NN}}^{\text{med},1} & : \psi_0^{(1)}(1^+, 0) = \psi_0^{(0)}(0^+, 1) + 0.25\psi_1^{(0)}(0^+, 1), \\
V_{\text{NN}}^{\text{med},3} & : \psi_0^{(1)}(1^+, 0) = \psi_0^{(0)}(1^+, 0) - 0.03\psi_1^{(0)}(1^+, 0), \\
V_{\text{NN}}^{\text{med},6} & : \psi_0^{(1)}(1^+, 0) = \psi_0^{(0)}(1^+, 0) - 0.25\psi_1^{(0)}(1^+, 0).
\end{aligned} \tag{38}$$

A full treatment shows that $V_{\text{NN}}^{\text{med},3}$ alone has little effect on the ground state wavefunction of ^{14}N and in fact actually decreases the strength in the $|33; 1^+0\rangle$ component of the wavefunction. Therefore, the strong short-distance repulsion generated by the three-nucleon contact interaction is the dominant term contributing to the suppression the Gamow-Teller transition matrix element.

$$J^\pi = 0^+, T = 1 \quad (n = n_0)$$

	$\langle 22 V_{\text{Chiral}}^{\text{med}} 22\rangle$	$\langle 22 V_{\text{Chiral}}^{\text{med}} 33\rangle$	$\langle 33 V_{\text{Chiral}}^{\text{med}} 33\rangle$
1	3.88	0.80	3.32
2	-3.18	-0.71	-2.68
3	2.15	0.32	1.92
4	-0.56	-0.12	-0.47
5	-0.89	-0.64	-0.44
6	1.75	1.24	0.88

Table 6: Matrix elements (in units of MeV) between $0p^{-2}$ states coupled to $(J^\pi, T) = (0^+, 1)$ for the six density-dependent contributions to the in-medium chiral nuclear interaction at nuclear matter saturation density n_0 .

In the BRS Bonn-B potential one might expect analogously that the scaling of the ω -meson mass plays a similar role. We therefore have performed a similar calculation using a BRS Bonn-B potential with no ω -meson mass scaling. In Fig. 12 we have plotted the $B(GT)$ values of the ground state to ground state transition using medium-modified interactions with the short-distance repulsion removed (the three-body contact term in the case of the in-medium chiral interaction and the dropping ω meson mass in the case of the BRS Bonn-B potential). We find that in both cases there is in fact a strong enhancement of the Gamow-Teller transition. Therefore, despite the fact that these two density-dependent interactions are behaving very differently at long distances (as inferred from the low-momentum components of their interactions in Figs. 4 and 7), they both include a strong short-distance repulsion that dramatically suppresses the Gamow-Teller transition matrix element.

$$J^\pi = 1^+, T = 0 \quad (n = n_0)$$

n/n_0	$\langle 22 V_{\text{Chiral}}^{\text{med}} 22 \rangle$	$\langle 23 V_{\text{Chiral}}^{\text{med}} 22 \rangle$	$\langle 23 V_{\text{Chiral}}^{\text{med}} 23 \rangle$	$\langle 23 V_{\text{Chiral}}^{\text{med}} 33 \rangle$	$\langle 22 V_{\text{Chiral}}^{\text{med}} 33 \rangle$	$\langle 33 V_{\text{Chiral}}^{\text{med}} 33 \rangle$
1	4.25	-0.65	1.67	2.14	-1.67	3.28
2	-3.15	0.73	-1.47	-1.44	1.47	-2.65
3	1.36	-0.76	1.53	0.00	-0.86	1.70
4	-0.54	0.13	-0.27	-0.23	0.25	-0.47
5	-0.47	0.56	-1.02	0.100	0.14	-0.35
6	1.04	-1.09	1.73	-0.01	-0.55	0.88

Table 7: Matrix elements (in units of MeV) between $0p^{-2}$ states coupled to $(J^\pi, T) = (1^+, 0)$ for the six density-dependent contributions to the in-medium chiral nuclear interaction at nuclear matter saturation density n_0 .

5 Summary and Conclusions

We have studied the effect of density-dependent low-momentum nucleon-nucleon interactions on the beta decay lifetime of ^{14}C . The in-medium chiral nuclear interaction was obtained from the leading-order three-nucleon force by contracting one pair of external lines and summing over the filled Fermi sea of nucleons, whereas the Brown-Rho-scaled Bonn-B potential was obtained by decreasing the masses and form factor cutoffs of the vector mesons and treating microscopically effective σ meson exchange as correlated two-pion exchange. Although both density-dependent interactions introduce additional strong repulsion at short distances, they differ largely at intermediate and long distances. The Brown-Rho scaled Bonn-B potential enhances the attraction at these distances (through a decreasing “ σ ” meson mass), but the Pauli-blocked two-pion exchange diagram obtained from the long-range chiral three-nucleon force is strongly repulsive in this region. Nevertheless, we find that in both models of the in-medium nuclear interaction the ground state to ground state Gamow-Teller transition strength is strongly suppressed at high densities. In contrast, the GT strengths from the ground state of ^{14}N to the excited states of ^{14}C exhibit only a small density dependence. From perturbative considerations we have found that, in general, short-range repulsive interactions lead to a strong suppression of the ground state to ground state transition. Moreover, we have explicitly removed the source of short-range repulsion in both interactions and found that this leads rather to an enhancement of the Gamow-Teller strength. We therefore suggest that the common short-distance behavior of these two interactions is responsible for their qualitatively similar effects on the beta decay lifetime of ^{14}C .

The authors of this work represent three generations of former students and postdocs who have been immensely inspired by Gerry Brown’s physics intuition and ideas. We gratefully dedicate this paper to Gerry on the occasion of his 85th birthday.

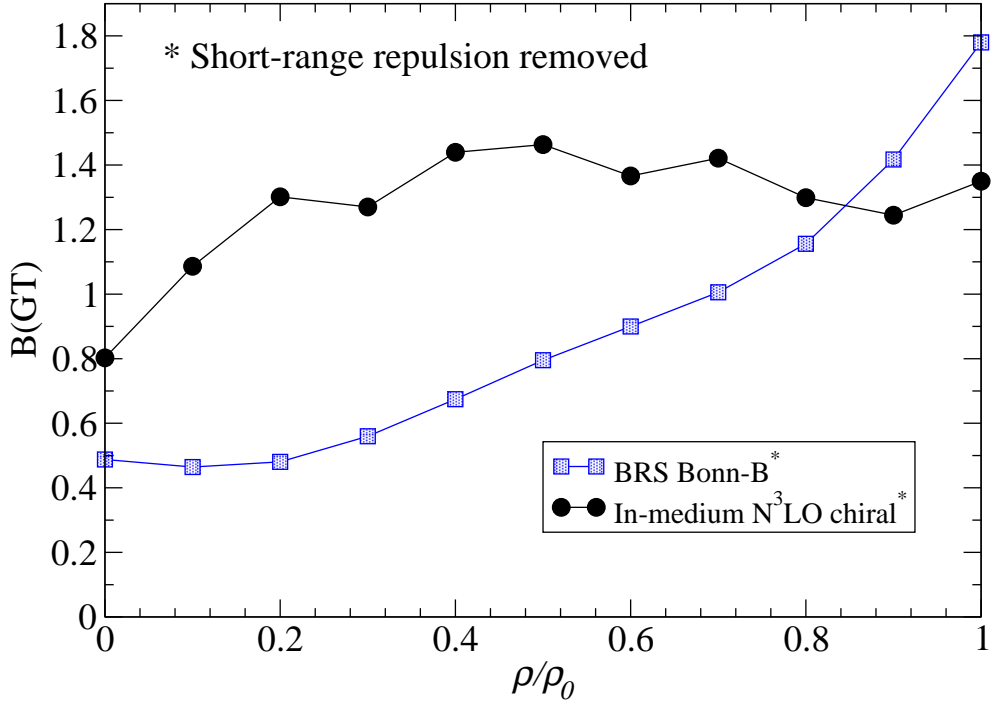


Figure 12: The $B(GT)$ values for the ^{14}C ground state to ^{14}N ground state transition as a function of the density for the medium-modified Bonn-B potential and the in-medium chiral nucleon-nucleon potential. The asterisk denotes that the additional density-dependent short-range repulsion has been removed from both potentials: the ω meson scaling in the case of the MM Bonn-B potential and the short-range contact three-nucleon force proportional to c_E in the in-medium chiral interaction.

6 Appendix: Explicit expressions for the Fermi sphere integrals in V_{NN}^{med}

In this appendix we tabulate the different functions that contribute to the density-dependent expressions in eqs. (6)-(12). The functions $\Gamma_j(p)$ result from Fermi sphere integrals over a single static pion propagator and have the explicit forms:

$$\Gamma_0(p) = k_f - m_\pi \left[\arctan \frac{k_f + p}{m_\pi} + \arctan \frac{k_f - p}{m_\pi} \right] + \frac{m_\pi^2 + k_f^2 - p^2}{4p} \ln \frac{m_\pi^2 + (k_f + p)^2}{m_\pi^2 + (k_f - p)^2}, \quad (39)$$

$$\Gamma_1(p) = \frac{k_f}{4p^2} (m_\pi^2 + k_f^2 + p^2) - \Gamma_0(p) - \frac{1}{16p^3} [m_\pi^2 + (k_f + p)^2] [m_\pi^2 + (k_f - p)^2] \ln \frac{m_\pi^2 + (k_f + p)^2}{m_\pi^2 + (k_f - p)^2}, \quad (40)$$

$$\Gamma_2(p) = \frac{k_f^3}{9} + \frac{1}{6} (k_f^2 - m_\pi^2 - p^2) \Gamma_0(p) + \frac{1}{6} (m_\pi^2 + k_f^2 - p^2) \Gamma_1(p), \quad (41)$$

$$\Gamma_3(p) = \frac{k_f^3}{3p^2} - \frac{m_\pi^2 + k_f^2 + p^2}{2p^2} \Gamma_0(p) - \frac{m_\pi^2 + k_f^2 + 3p^2}{2p^2} \Gamma_1(p). \quad (42)$$

The $G_j(p, q)$ functions result from Fermi sphere integrals over the product of two static pion propagators. Angular integrations are performed analytically, and the remaining relevant momentum integrals are given by

$$G_{0,*,**}(p, q) = \frac{2}{q} \int_0^{k_f} dk \frac{\{k, k^3, k^5\}}{\sqrt{A(p) + q^2 k^2}} \ln \frac{qk + \sqrt{A(p) + q^2 k^2}}{\sqrt{A(p)}}, \quad (43)$$

where $A(p) = [m_\pi^2 + (k + p)^2][m_\pi^2 + (k - p)^2]$. The remaining functions $G_j(p, q)$ are related to those above through the equations

$$G_1(p, q) = \frac{\Gamma_0(p) - (m_\pi^2 + p^2)G_0(p, q) - G_*(p, q)}{4p^2 - q^2}, \quad (44)$$

$$G_{1*}(p, q) = \frac{3\Gamma_2(p) + p^2\Gamma_3(p) - (m_\pi^2 + p^2)G_*(p, q) - G_{**}(p, q)}{4p^2 - q^2}, \quad (45)$$

$$G_2(p, q) = (m_\pi^2 + p^2)G_1(p, q) + G_*(p, q) + G_{1*}(p, q), \quad (46)$$

$$G_3(p, q) = \frac{\frac{1}{2}\Gamma_1(p) - 2(m_\pi^2 + p^2)G_1(p, q) - 2G_{1*}(p, q) - G_*(p, q)}{4p^2 - q^2}. \quad (47)$$

In this chain of equations the functions indexed with an asterisk play only an auxiliary role for the construction of $G_{1,2,3}(p, q)$. We note that all functions $G_j(p, q)$ are non-singular at $q = 2p$ (corresponding to scattering in backward direction). For notational simplicity, the k_f -dependence of $\Gamma_j(p)$ and $G_j(p, q)$ has been suppressed.

References

- [1] S. Weinberg, Phys. Lett. B **251** (1990) 288.
- [2] S. Weinberg, Nucl. Phys. **B363** (1991) 3.
- [3] C. Ordonez and U. van Kolck, Phys. Lett. B **291** (1992) 459.
- [4] N. Kaiser, R. Brockmann, and W. Weise, Nucl. Phys. **A625** (1997) 758.

- [5] E. Epelbaum, W. Glöckle, and U.-G. Meißner, Nucl. Phys. **A637** (1998) 107.
- [6] N. Kaiser, Phys. Rev. C **64** (2001) 057001.
- [7] N. Kaiser, Phys. Rev. C **65** (2001) 017001.
- [8] D. R. Entem and R. Machleidt, *Phys. Rev. C* **66** (2002) 014002.
- [9] D. R. Entem and R. Machleidt, *Phys. Rev. C* **68** (2003) 041001(R).
- [10] E. Epelbaum, *Prog. Part. Nucl. Phys.* **57** (2006) 654.
- [11] C. Adami, T. Hatsuda and I. Zahed, Phys. Rev. D **43** (1991) 921.
- [12] G. E. Brown and M. Rho, Phys. Rev. Lett. **66** (1991) 2720.
- [13] T. Hatsuda and S. H. Lee, Phys. Rev. C **46** (1992) R34.
- [14] G. E. Brown and M. Rho., Phys. Rept. **269** (1996) 333.
- [15] R. Rapp and J. Wambach, Adv. Nucl. Phys. **25** (2000) 1.
- [16] R. Rapp, J. Wambach and H. van Hees, arXiv:0901.3289.
- [17] M. Lutz, S. Klimt and W. Weise, Nucl. Phys. **A542** (1992) 521.
- [18] E. G. Drukarev and E. M. Levin, Nucl. Phys. **A511** (1990) 679; **A516**, (1990) 715.
- [19] N. Kaiser, P. de Homont, and W. Weise, Phys. Rev. C **77** (2008) 025204.
- [20] M. Bando, T. Kugo and K. Yamawaki, Phys. Rept. **164** (1988) 217.
- [21] M. Harada and K. Yamawaki, Phys. Rept. **381** (2003) 1.
- [22] G. E. Brown, H. Müther and M. Prakash, Nucl. Phys. **A506** (1990) 565.
- [23] R. Rapp, R. Machleidt, J. W. Durso and G. E. Brown, Phys. Rev. Lett. **82** (1999) 1827.
- [24] J. W. Holt, G. E. Brown, J. D. Holt and T. T. S. Kuo, Nucl. Phys. **A785** (2007) 322.
- [25] J. W. Holt, G. E. Brown, T. T. S. Kuo, J. D. Holt and R. Machleidt, Phys. Rev. Lett. **100**, (2008) 062501.
- [26] L.-W. Siu, J. W. Holt, T. T. S. Kuo and G. E. Brown, Phys. Rev. C **79** (2009) 054004.
- [27] S. Leupold, V. Metag and U. Mosel, Int. J. Mod. Phys. E **19** (2010) 147.
- [28] F. Klingl, N. Kaiser and W. Weise, Nucl. Phys. **A624** (1997) 527.
- [29] M. Post and U. Mosel, Nucl. Phys. **A688** (2001) 808.
- [30] W. Peters, M. Post, H. Lenske, S. Leupold and U. Mosel, Nucl. Phys. **A632** (1998) 109.
- [31] R. Rapp and J. Wambach, Adv. Nucl. Phys. **25** (2000) 1.
- [32] A. Nogga, H. Kamada, and W. Glöckle, Phys. Rev. Lett. **85** (2000) 944.
- [33] S. C. Pieper, K. Varga, and R. B. Wiringa, Phys. Rev. C **66** (2002) 044310.

- [34] P. Navrátil, V. G. Gueorguiev, J. P. Vary, W. E. Ormand, and A. Nogga, *Phys. Rev. Lett.* **99** (2007) 042501.
- [35] B. D. Day, *Rev. Mod. Phys.* **39** (1967) 719.
- [36] H. Q. Song, M. Baldo, G. Giansiracusa, and U. Lombardo, *Phys. Rev. Lett.* **81** (1998) 1584.
- [37] I. E. Lagaris and V. R. Pandharipande, *Nucl. Phys.* **A359** (1981) 331; **A359** (1981) 349.
- [38] S. D. Yang, J. Heyer, and T. T. S. Kuo, *Nucl. Phys.* **A448** (1986) 420.
- [39] R. B. Wiringa, V. Fiks, and A. Fabrocini, *Phys. Rev. C* **38** (1988) 1010.
- [40] N. Sakamoto *et al.*, *Phys. Lett. B* **367** (1996) 60.
- [41] H. Sakai *et al.*, *Phys. Rev. Lett.* **84** (2000) 5288.
- [42] H. Witala, W. Glöckle, D. Hüber, J. Golak, and H. Kamada, *Phys. Rev. Lett.* **81** (1998) 1183.
- [43] S. Nemoto, K. Chmielewski, S. Oryu, and P. U. Sauer, *Phys. Rev. C* **58** (1998) 2599.
- [44] J. W. Holt, N. Kaiser, and W. Weise, *Phys. Rev. C* **79** (2009) 054331.
- [45] D. R. Inglis, *Rev. Mod. Phys.* **25** (1953) 390.
- [46] B. Jancovici and I. Talmi, *Phys. Rev.* **95** (1954) 289.
- [47] E. Epelbaum, H.-W. Hammer, and U.-G. Meißner, *Rev. Mod. Phys.* **81** (2010) 1773.
- [48] R. Machleidt, *Phys. Rev. C* **63** (2001) 024001.
- [49] V. G. J. Stoks, R. A. M. Klomp, C. P. F. Terheggen, and J. J. de Swart, *Phys. Rev. C* **49** (1994) 2950.
- [50] R. B. Wiringa, V. G. J. Stoks, and R. Schiavilla, *Phys. Rev. C* **51** (1995) 38.
- [51] M. C. M. Rentmeester, R. G. E. Timmermans, and J. J. de Swart, *Phys. Rev. C* **67** (2003) 044001.
- [52] E. Epelbaum, A. Nogga, W. Glöckle, H. Kamada, U.-G. Meißner, and H. Witala, *Phys. Rev. C* **66** (2002) 064001.
- [53] A. Nogga, P. Navratil, B. R. Barrett, and J. P. Vary, *Phys. Rev. C* **73** (2006) 064002.
- [54] S. K. Bogner, T. T. S. Kuo, L. Coraggio, A. Covello, and N. Itaco, *Phys. Rev. C* **65** (2002) 051301(R).
- [55] S. K. Bogner, T. T. S. Kuo, and A. Schwenk, *Phys. Rep.* **386** (2003) 1.
- [56] A. Nogga, S. K. Bogner, and A. Schwenk, *Phys. Rev. C* **70** (2004) 061002(R).
- [57] J. W. Holt, N. Kaiser and W. Weise, *Phys. Rev. C* **81** (2010) 024002.
- [58] N. Kaiser, R. Brockmann, and W. Weise, *Nucl. Phys.* **A625** (1997) 758.

- [59] S. K. Bogner, A. Schwenk, R. J. Furnstahl, and A. Nogga, *Nucl. Phys.* **A763** (2005) 59.
- [60] B. A. Campbell, J. Ellis and K. A. Olive, *Nucl. Phys.* **B345** (1990) 57.
- [61] K. Suzuki *et al.*, *Phys. Rev. Lett.* **92** (2004) 072302.
- [62] E. E. Kolomeitsev, N. Kaiser and W. Weise, *Phys. Rev. Lett.* **90** (2003) 092501.
- [63] M. Gell-Mann, R. J. Oakes and B. Renner, *Phys. Rev.* **175** (1968) 2195.
- [64] T. D. Cohen, R. J. Furnstahl and D. K. Griegel, *Phys. Rev. Lett.* **67** (1991) 961.
- [65] J. Gasser, H. Leutwyler and M. E. Sainio, *Phys. Lett.* **B253** (1991) 252.
- [66] Y. Kwon, M. Procura and W. Weise, *Phys. Rev. D* **78** (2008) 055203.
- [67] M. Post and U. Mosel, *Nucl. Phys.* **A699** (2002) 169.
- [68] B. Friman and H. J. Pirner, *Nucl. Phys.* **A617** (1997) 496.
- [69] H.-C. Kim, J. W. Durso and K. Holinde, *Phys. Rev. C* **49** (1994) 2355.
- [70] M. Rho, *Phys. Rev. Lett.* **54** (1985) 767.
- [71] R. Machleidt, *Adv. Nucl. Phys.* **19** (1989) 189.
- [72] F. Ajzenberg-Selove, J. H. Kelley, and C. D. Nesaraja, *Nucl. Phys.* **A523** (1991) 1.
- [73] L. Zamick, *Phys. Lett.* **21** (1966) 194.
- [74] S. Aroua, P. Navrátil, L. Zamick, M. S. Fayache, B. R. Barrett, J. P. Vary, and K. Heyde, *Nucl. Phys.* **A720** (2003) 71-83.
- [75] L. A. Schaller, L. Schellenberg, A. Ruetschi, and H. Schneuwly, *Nucl. Phys.* **A343** (1980) 333.
- [76] W. Schütz, *Z. Phys.* **A273** (1975) 69.
- [77] P. Navrátil, J. P. Vary, B. R. Barrett, *Phys. Rev. C* **62** (2000) 054311.
- [78] S. C. Pieper and R. B. Wiringa, *Ann. Rev. Nucl. Part. Sci.* **51** (2001) 53.
- [79] T. T. S. Kuo and E. Osnes, *Lecture Notes in Physics Vol. 364* (Springer-Verlag, New York, 1990).
- [80] M. Hjorth-Jensen, T. T. S. Kuo, and E. Osnes, *Phys. Rep.* **261**, 126 (1995), and references therein.
- [81] A. Arima and L. J. Huang-Lin, *Phys. Lett.* **B41** (1972) 429; **B41** (1972) 435.
- [82] B. Castel and I. S. Towner, *Modern Theories of Nuclear Moments* (Clarendon Press, Oxford, 1990).
- [83] I. S. Towner, *Phys. Rept.* **155** (1987) 263.
- [84] B. A. Brown and B. H. Wildenthal, *Nucl. Phys.* **A474** (1987) 290.
- [85] A. Negret *et al.*, *Phys. Rev. Lett.* **97** (2006) 062502.